

8-2016

Novel gain enhancement technique for microstrip patch antennas based on multi-pronged feed network synthesis

Brian J. Vaughn
Purdue University

Follow this and additional works at: https://docs.lib.purdue.edu/open_access_theses



Part of the [Electrical and Computer Engineering Commons](#)

Recommended Citation

Vaughn, Brian J., "Novel gain enhancement technique for microstrip patch antennas based on multi-pronged feed network synthesis" (2016). *Open Access Theses*. 1015.
https://docs.lib.purdue.edu/open_access_theses/1015

This document has been made available through Purdue e-Pubs, a service of the Purdue University Libraries. Please contact epubs@purdue.edu for additional information.

**PURDUE UNIVERSITY
GRADUATE SCHOOL
Thesis/Dissertation Acceptance**

This is to certify that the thesis/dissertation prepared

By Brian Vaughn

Entitled Novel Gain Enhancement Technique for Microstrip Patch Antennas Based On Multi-Pronged Feed Network Synthesis

For the degree of Master of Science in Electrical and Computer Engineering

Is approved by the final examining committee:

DIMITRIOS PEROULIS

DAVID J. LOVE

KEVIN J. WEBB

MICHAEL D. ZOLTOWSKI

To the best of my knowledge and as understood by the student in the Thesis/Dissertation Agreement, Publication Delay, and Certification/Disclaimer (Graduate School Form 32), this thesis/dissertation adheres to the provisions of Purdue University's "Policy on Integrity in Research" and the use of copyrighted material.

DIMITRIOS PEROULIS

Approved by Major Professor(s): _____

Approved by: V. Balakrishnan

05/31/2016

Head of the Department Graduate Program

Date

NOVEL GAIN ENHANCEMENT TECHNIQUE FOR MICROSTRIP PATCH
ANTENNAS BASED ON MULTI-PRONGED FEED NETWORK SYNTHESIS

A Thesis

Submitted to the Faculty

of

Purdue University

by

Brian J. Vaughn

In Partial Fulfillment of the

Requirements for the Degree

of

Master of Science in Electrical and Computer Engineering

August 2016

Purdue University

West Lafayette, Indiana

This thesis is dedicated to Taryn Vaughn, Katrina Ray, and Sara Baldwin. Thanks for always listening.

ACKNOWLEDGEMENTS

A special thanks to Dr. Dimitrios Peroulis, whose guidance and understanding always kept me on track. The author would also like to thank Mark Hickle for his valuable advice and insight.

TABLE OF CONTENTS

	Page
LIST OF TABLES.....	vii
LIST OF FIGURES.....	viii
ABSTRACT	x
1. INTRODUCTION	1
1.1 Overview	1
1.2 Thesis Structure	2
2. SUPERGAIN ANTENNA PRINCIPLES	3
2.1 Supergain Methodology	3
2.2 Detriments of Supergain.....	4
2.3 Modification of Supergain Paradigm	5
2.3.1 Modification 1: Replacing Arrays With Single Modified Topology	5
2.3.2 Modification 2: Tuned Feed Network Appendage	5
3. ENHANCED GAIN PATCH ANTENNA THEORY	6
3.1 Rectangular Patch Antenna Cavity Model	6
3.1.1 Wave Equation and Field Solutions	7
3.1.2 Custom Mode Excitation.....	9
3.2 Rectangular Patch Antenna Radiation Properties.....	10
3.2.1 Equivalent Magnetization Currents and Far-Field Radiation Integrals.....	11
3.2.2 Enhanced Gain Patch Directivity	15
3.3.Modified Mode Approximation Through Voltage Boundary Conditions	19
3.3.1 Cavity Mode Voltage Profile	19

	Page
3.3.2 Multi-Pronged Feed Network Superposition	20
3.4. Conclusions	22
4. ENHANCED GAIN PATCH ANTENNA FEED DESIGN	23
4.1. Tuned Transmission Line Network Formulation	23
4.1.1 Z-Matrix Analysis and Port Parameter Definitions	24
4.1.2 Voltage Ratio Transformation Analysis and Locked DPI Assumption	27
4.1.3 Transmission Line Parameter Definition.....	29
4.2 Matching Network Design	31
4.2.1 Stage 1: High Impedance Line Section	32
4.2.2 Stage 2: Quarter-Wave Transformer.....	32
4.3 Conclusions	33
5. ENHANCED GAIN PATCH DESIGN WORKFLOW.....	34
5.1 Step 1: Substrate and Patch Dimension Definition	34
5.2 Step 2: Voltage Profile Definition	35
5.3 Step 3: Z-Matrix Extraction	35
5.4 Step 4: Initial Feed Network Definition.....	36
5.5 Step 5: Initial Feed Network Implementation and Tweaking.....	36
5.6 Step 6: Matching Network Design	37
5.7 Conclusions	38
6. PROTOTYPE DESIGNS AND RESULTS.....	39
6.1 Prototype Dimensions	39
6.2 Measurement Results	41
6.2.1 Prototype 1 Results.....	41
6.2.2 Prototype 2 Results.....	43

	Page
6.2.3 Prototype 3 Results.....	44
6.2.4 Prototype 4 Results.....	46
6.2.5 Reference Patch Comparison and Additional Results.....	47
6.3 Results and Design Tradeoff Discussion.....	49
6.4 Conclusions.....	50
7. CONCLUSIONS AND FUTURE WORK.....	51
7.1 Enhanced Gain Patch Pattern and Form Factor Refinement.....	51
7.2 Other Antenna Types.....	55
7.3 Conclusions.....	55
LIST OF REFERENCES.....	56
APPENDICES	
A. Amplitude Ratio Directivity Plot Creation Code.....	57
B. Feed Network Synthesis Code.....	62

LIST OF TABLES

Table	Page
6.1 Prototype Dimensions.....	40
6.2 Additional Prototype Results	49

LIST OF FIGURES

Figure	Page
2.1 Supergain Example.....	4
3.1 Patch Cavity Coordinate System Diagram.....	7
3.2 Directivity vs. Amplitude Ratio Plot.....	18
3.3 Feed Network Example.....	20
4.1 Feed Network Example (same as 3.3).....	24
4.2 Full Feed Network Circuit.....	33
5.1 Z-Parameter Extraction Scheme.....	35
5.2 Initial Feed Network (same as 3.3).....	36
6.1 Prototype Dimension Diagram.....	39
6.2 Reference Patch Dimensions.....	40
6.3 Prototype #1 Circuit.....	41
6.4 Prototype #1 3-D Pattern.....	42
6.5 Prototype #1 Return Loss.....	42
6.6 Prototype #2 Circuit.....	43
6.7 Prototype #2 3-D Pattern.....	43
6.8 Prototype #2 Return Loss.....	44
6.9 Prototype #3 Circuit.....	44
6.10 Prototype #3 3-D Pattern.....	45
6.11 Prototype #3 Return Loss.....	45
6.12 Prototype #4 Circuit.....	46
6.13 Prototype #4 3-D Pattern.....	46
6.14 Prototype #4 Return Loss.....	47
6.15 Reference Patch Circuit.....	47

Figure	Page
6.16 Reference Patch 3-D Pattern.....	48
6.17 Reference Patch Return Loss.....	48
7.1 Refined Patch Design Top View	52
7.2 Refined Patch Design Bottom View	52
7.3 Refined Patch Design Expanded View	53
7.4 Refined Patch Design Simulated 3-D Pattern.....	53
7.5 Refined Patch Design Simulated Return Loss.....	54

ABSTRACT

Vaughn, Brian J. M.S., Purdue University, August 2016. Novel Gain Enhancement Technique for Microstrip Patch Antennas Based on Multi-Pronged Feed Network Synthesis. Major Professor: Dimitrios Peroulis

Developing antennas with enhanced gain has always been an important pursuit within the antenna community, as a higher gain leads to an increase in the received power for any given wireless link. In general, when a higher gain is needed for an application, only certain types of antennas can be used. The goal of this thesis project was to develop a method for increasing the gain of antennas that already exist by applying modifications to them, expanding the design flexibility for wireless applications. In this thesis, a novel method for increasing the gain of microstrip patch antennas by synthesizing specialized multi-branch feed networks is developed and verified experimentally. A full theoretical foundation based on cavity modal and radiation analysis is discussed followed by a detailed explanation of the feed network design, which culminates in the presentation of a start-to-finish full design workflow using MATLAB and ANSYS HFSS simulation. Four prototypes that were designed using this methodology are also presented, along with results that demonstrate the method's efficacy as well as its tradeoffs. In addition, the MATLAB codes used in the design process are given, allowing the thesis to be used as a design guide.

1. INTRODUCTION

1.1. Overview

As the importance of wireless technology in our society grows, so too does the importance of antenna performance. More specifically, the ability of a system to send a sufficient amount of power to a receiver device in all applications ranging from communications to wireless power transfer depends on the gain of the transmission system's antenna. While the antenna is not the only crucial component of a wireless system, it effectively defines the range and received power of any wireless link, and since free space path loss for electromagnetic signals at microwave and radio frequencies is notoriously high (even without obstructions or varying transmission media), power efficiency in transmission systems becomes an essential parameter. For this reason, developing antennas with higher gain is a priority in the antenna community.

Of course, the gain of an antenna system can usually be improved by choosing larger antenna types, or by implementing antenna arrays to increase the gain via superposition effects. This, however, comes with the trade-off of raising the size requirements of the allotted antenna space using specific antenna structures, and in some cases, this may not be possible or preferable. This thesis focuses on modifying known antenna topologies to enhance their gain without increasing the sizing requirements the same way larger antenna types and arrays require. This is accomplished through a novel radiator and feed network design methodology that takes ideas from traditional supergain antenna array theory and ultimately yields feasible implementations. The focus here is placed on microstrip patch antennas, but the principles developed here can be extrapolated to other antennas with similar radiation characteristics.

1.2.Thesis Structure

This thesis will be split into seven chapters, including the introduction. Chapter 2 will be a summary of supergain principles. Chapter 3 will narrow the supergain idea to patch antennas and define the foundational theory for this work. Chapter 4 will detail the feed network design process to obtain enhanced gain characteristics. Chapter 5 will detail the start to finish workflow of designing supergain patch antennas. Chapter 6 will show the design, fabrication, and testing of the prototypes developed for this project, as well as the results and trade-off discussion, and finally, chapter 7 will focus on conclusions drawn and future directions for the research.

2. SUPERGAIN ANTENNA PRINCIPLES

Supergain antenna array theory is not new. In 1943, Schelkunoff showed that the gain of an end-fire antenna array has no theoretical limit for a given element spacing [1]. Since then, several others have launched their own investigations into the validity and feasibility of his claims [2-5]. The point of supergain array design is to take an allotted design space for an antenna system (such as the space where the elements of a linear array are placed) and modify the excitation scheme to increase the array's directivity without changing its overall size. This is generally done by raising the number of elements in the array, decreasing the spacing between them, and changing the excitations accordingly. This does not come without cost, however, as will be detailed below.

2.1. Supergain Methodology

Supergain array design is based upon the assumption that normal excitation schemes (such as for example, that of a uniform phased array) do not provide the highest directivity possible for a given total array size. If one is to think of, say, a linear array as a discrete sampling of a linear current distribution that yields a certain pattern in space, then designing a supergain array would mean changing the excitations to sample a current distribution that will give a higher than normal directivity for a given array size. Fig. 2.1. Illustrates how this would be done for such a linear array.

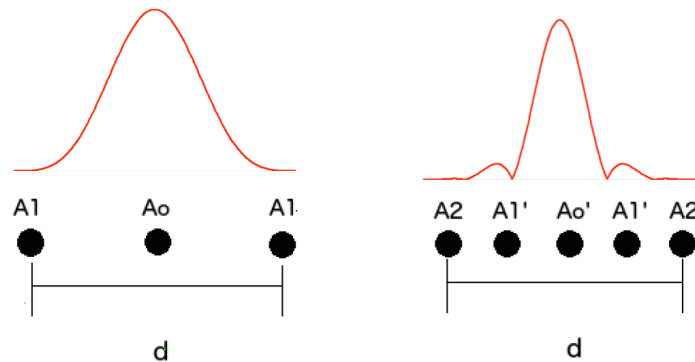


Fig. 2.1: Modification of linear array to achieve supergain

How the new excitations are derived is based on the designer. Yaru designed an array with $\lambda/32$ inter-element spacing using well-documented Chebyshev array theory [2]. It is also possible to define an excitation scheme by specifying a desired far-field pattern and deriving the current distribution that matches this pattern with algorithms such as the method of moments (MoM). Either way, finding the required excitations is not particularly difficult or novel. However, pursuing this method has significant drawbacks.

2.2. Detriments of Supergain

As noted by Yaru and Haviland, designing a supergain array requires excitations that become more and more unfeasible the more elements one adds or the smaller the inter-element spacing becomes [2,4]. More specifically, the required supergain excitation amplitudes become prohibitively large and the required precision in these amplitudes becomes prohibitively high when the limits of the directivity are pushed. This results in unrealizable systems, be it because the required precision cannot be attained, the required amplitudes cannot be reached, or because the efficiency of such a system would plummet due to ohmic loss if the two former issues were addressed. For these reasons, the problem of supergain arrays has not been solved on a large scale. However, this thesis details an offshoot of the supergain paradigm that does not have the problems mentioned above, but still results in significant gain enhancement. It should be noted that the directivity this

offshoot method affords is not limitless like in the supergain case, but it leads to realizable antenna designs.

2.3.Modification of Supergain Paradigm

The novel modifications made to the supergain paradigm in this work are as follows:

2.3.1.Modification 1: Replacing Arrays With Single Modified Topology

The first modification involves straying away from traditional arrays when thinking about supergain and replacing them with single radiators with modifications applied to them. If this is done, the problem of inter-element spacing now becomes one of structure dimensions. This modification allows for increased customization in the antenna design and also allows us to circumnavigate the precision and excitation magnitude limitations that plague normal supergain design. Instead of designing an array that must compensate for reduced spacing or a higher number of elements, the structures developed in this thesis will begin with a known topology (i.e., the patch antenna) and simply add to it to tune its radiation pattern without forcing the structure to require unfeasible excitations, leading to practical topologies.

2.3.2.Modification 2: Tuned Feed Network Appendage

In this work, each antenna design presented will have one feed line to be connected to a transmitter, but this feed will split into several lines and connect to the primary radiator in several places. This is analogous to a corporate feed structure, only each branch connects to the same antenna and this feed has a role beyond that of a simple feed structure. The reason for this will become clear in chapter 3, but it involves forcing the radiator to imitate voltage/current distributions needed to increase the gain beyond normal limits. From now on, only rectangular microstrip patch antennas will be specifically considered and discussed regarding this modified paradigm. In the following chapter, the theory behind patch antenna gain enhancement will be developed and discussed.

3. ENHANCED GAIN PATCH ANTENNA THEORY

This chapter, using the microstrip patch antenna as a basis, will establish the theoretical framework for the proposed gain enhancement method. It will begin by defining the modal characteristics of the antennas by examining the cavity model for patches, after which, the radiation properties will be derived. From there, the foundation for the modifications presented in chapter 2 will be built, culminating in a full theoretical model for the enhanced gain patch antenna from a modal point of view.

3.1. Rectangular Patch Antenna Cavity Model

According to Balanis, when a thin conductor (i.e., the patch) is placed on a substrate above a ground plane and energized, electric forces effectively prevent the majority of the currents on the patch to running to patch's top surface from the patch's bottom surface [6]. While such currents are not exactly zero in reality, they are small enough (given how thin the patch conductors typically are) that we may neglect their effects, and since the currents are effectively zero under this approximation, we may conclude that the tangential magnetic fields at the patch edges are approximately zero. This means we may define magnetic wall boundary conditions on the patch edges, allowing us to obtain a field solution from Maxwell's Equations. What follows is a summary of the derivation of this field solution. A more detailed and complete treatment may be found in Balanis 14.2.2 [6].

3.1.1. Wave Equation and Field Solutions

Fig. 3.1 illustrates the profile and coordinate system layout to be used for the cavity model with patch dimensions L , W , and h .

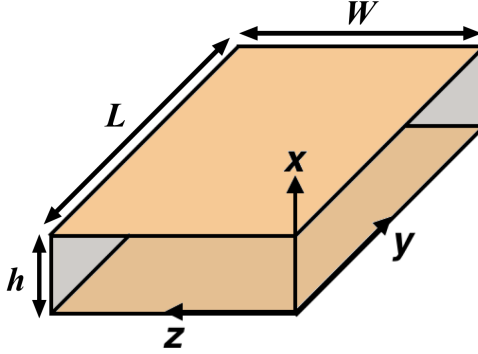


Fig. 3.1: Cavity model layout diagram

Under this model, it can be shown that the vector potential A within the only has an x -component and obeys the wave equation given by

$$\nabla^2 A_x + k^2 A_x = 0 \quad (3.1)$$

Using separation of variables, the general solution for the vector potential takes the following form [6]:

$$A_x = [A_1 \cos(k_x x) + B_1 \sin(k_x x)] * [A_2 \cos(k_y y) + B_2 \sin(k_y y)] * [A_3 \cos(k_z z) + B_3 \sin(k_z z)] \quad (3.2)$$

Where A_n and B_n are amplitude coefficients, x , y , and z are cavity coordinates, and k_x , k_y , and k_z are wave number parameters to be defined by the boundary conditions. Given the relationships between A_x and the E and H fields that arise from the definition of the vector potential and Maxwell's Equations, along with the boundary conditions for the E and

H tangential components at the cavity walls, it can be shown that A_x , E_x , and the H -fields take the final form as follows [6]:

$$A_x = A_{mnp} \cos(k_x x) \cos(k_y y) \cos(k_z z) \quad (3.3a)$$

$$E_x = -j \frac{k^2 - k_x^2}{\omega \epsilon \mu} A_{mnp} \cos(k_x x) \cos(k_y y) \cos(k_z z) \quad (3.3b)$$

$$H_x = 0 \quad (3.3c)$$

$$H_y = -\frac{k_z}{\mu} A_{mnp} \cos(k_x x) \cos(k_y y) \sin(k_z z) \quad (3.3d)$$

$$H_z = \frac{k_y}{\mu} A_{mnp} \cos(k_x x) \sin(k_y y) \cos(k_z z) \quad (3.3e)$$

with

$$k_x = \frac{m\pi}{h} \quad (3.4a)$$

$$k_y = \frac{n\pi}{L} \quad (3.4b)$$

$$k_z = \frac{p\pi}{W} \quad (3.4c)$$

and

$$k_x^2 + k_y^2 + k_z^2 = k^2 = \omega^2 \epsilon \mu \quad (3.5)$$

Here, A_{mnp} is a general amplitude coefficient determined by the cavity excitation, ω is the angular frequency, ϵ and μ are the permittivity and permeability of the substrate, respectively, and m, n, p , are constants which can take any integer value greater than or equal to 0 (though they cannot all be zero at the same time). The latter values denote the index of the of the solution or “mode” in question. Note that in general, the y and z components of

the electric field are nonzero. However, from here on, only modes with $m = 0$ will be considered, and the E -field y and z components drop under this condition, so they have been neglected here. Also note that the modes here are transverse magnetic in the x direction (TM^x).

3.1.2. Custom Mode Excitation

From Eqn. 3.5, it can be seen that the single frequency any mode in the cavity can sustain is subject to the following condition:

$$f_{mnp} = \frac{1}{2\pi\sqrt{\epsilon\mu}} \sqrt{\left(\frac{m\pi}{h}\right)^2 + \left(\frac{n\pi}{L}\right)^2 + \left(\frac{p\pi}{W}\right)^2} \quad (3.6)$$

Based on the patch dimensions, the mode with the lowest resonant frequency is referred to as the “dominant” mode. For the sake of simplicity in analysis, patches are generally designed such that the TM^x₀₁₀ is the dominant mode (since this means that the E -field does not vary in the z direction) and all other modes are neglected. However, it will be shown through the enhanced gain model presented in this thesis that the modal excitation need not be identical to that of the TM^x₀₁₀ or any other individual mode if the right excitation conditions are met, and if enhanced gain is desired, the excited modal distribution must differ from any individual mode discussed thus far. However, within the scope of this thesis, this new distribution will only deviate from the TM^x₀₁₀ mode in its z dependence, i.e., it will retain the same y dependence as the TM^x₀₁₀ mode, but will not remain constant in z (why this is will become clear when the patch radiation is discussed). This z dependence will not match any other known individual mode either. The modified mode will from now on be referred to as the TM^x₀₁₀' mode since it will use the TM^x₀₁₀ mode as a base and the electric field of this modified mode will take the following form:

$$E_x^{010'} = -j\omega\cos\left(\frac{\pi y}{L}\right) [A_1 + A_2 f(z)] \quad (3.7)$$

Where $f(z)$ is an arbitrary function to be chosen during the design process and A_1 and A_2 are amplitude coefficients. Now, to be clear, it is not being claimed that any arbitrary electric field distribution can be sustained within the patch cavity alone. In fact, from what is known about the boundary conditions and the Uniqueness Theorem of Electromagnetics, this cannot be the case. However, $f(z)$ is essential to the enhanced gain patch formulation, and its full function and importance will be highlighted in the following sections, so we will assume the mode can take this form for now.

As a final note, referring to Eqn. 3.6, it is clear that the resonance condition for the TM^x_{010} mode only depends on L . Because of this, the frequency of operation may be chosen independently of W , making the patch width a degree of freedom in the design process. The TM^x_{010} ' mode will share this property, but it should be noted that the patch width will affect the distribution of this new mode. The width, however, will remain unrestricted. Again, more details will be made clear when the design process is further developed.

This concludes the development of the cavity model for the patch antenna. Next, the radiation properties of the antenna will be examined given the custom mode excitation.

3.2. Rectangular Patch Antenna Radiation Properties

The development of the radiation properties for the patch antenna relies heavily on the Field Equivalence Principle, which states that, given a finite surface region with a defined field distribution, this field may be replaced by an “equivalent” current source (either electric or magnetic) in the presence of a perfect electric or magnetic conductor without changing the radiated fields outside this region. From there, image theory may be used to get rid of the conductor and derive the radiated fields from the remaining current element. A full explanation of this process is provided in Balanis 12.2 [6]. The Field Equivalence Principle is especially useful when considering radiation from apertures, and this principle is used regarding patch antenna radiation because each sidewall (not includ-

ing the top and bottom electric conductor sidewalls) can be considered an aperture with a tangential electric field. This idea will be developed further in the following sections.

3.2.1. Equivalent Magnetization Currents and Far-Field Radiation Integrals

By the Field Equivalence Principle, any electric field tangential to an aperture surface may be replaced by a surface magnetization current \mathbf{M}_s via the following relation [6].

$$\mathbf{M}_s = -2 \hat{\mathbf{n}} \times \mathbf{E}_{\text{tan}} \quad (3.8)$$

This is to say that the equivalent magnetization current is -2 times cross product of the surface normal unit vector and the tangential E -field. This equation arises from a combination of surface boundary conditions and image theory. Once this current is known, expressions for the far field radiation may be derived using the integral solution to the wave equation involving the electric vector potential \mathbf{F} . In general, solving for the radiated electric field would also involve the magnetic vector potential \mathbf{A} , but under the assumptions of the field equivalence principle in this case, the electric current density \mathbf{J}_s is 0, so the magnetic vector potential drops.

Given the definition of the electric vector potential with no electric current source

$$\nabla \times \mathbf{F} = -\epsilon \mathbf{E} \quad (3.9)$$

along with the wave equation solution and the coordinate system defined in Fig. 3.1, closed form relations can be derived for the far-field radiated electric field from a patch cavity aperture. In general, there are four apertures to consider in the patch cavity. However, as detailed in Balanis 14.2.2, only the apertures with y directed normal vectors will radiate in the far field given the type of cavity mode being considered here [6]. The reason for this is that the equivalent magnetization currents for

the the other two slots are equal in magnitude, but out of phase, so they will thus cancel each other out in the most important radiation direction (the x direction) and be negligibly small in other directions. This will remain true regarding the $\text{TM}^{x_{010}}$ ' mode distribution if the corresponding $f(z)$ is chosen to be symmetric with respect to the patch center axis, i.e., if $f(z)$ is chosen such that its values at $z = 0$ and $z = W$ are equal in magnitude and sign.

Given that the two radiating slots have y directed normal vectors and the tangential electric fields on these apertures only have x components, the equivalent magnetization currents will be purely z directed. Knowing this, along with the rest of the information discussed, we may derive the electric vector potential and far zone electric field radiated from one of the cavity apertures (the one at $y = 0$ specifically) with respect to the $\text{TM}^{x_{010}}$ ' mode to obtain the following expressions:

$$\mathbf{M}_s = \hat{\mathbf{z}} 2j\omega [A_1 + A_2 f(z)] \quad (3.10)$$

$$\mathbf{E}_{rad} = \frac{1}{\varepsilon} \nabla \times \mathbf{F} \quad (3.11a)$$

$$\approx \frac{e^{-jkr}}{4\pi r} \nabla \times \iint_S \mathbf{M}_s e^{jkr' \cos\psi} ds' \quad (3.11b)$$

$$\approx \hat{\boldsymbol{\phi}} \frac{\omega k e^{-jkr}}{2\pi r} \int \int [A_1 + A_2 f(z)] \sin\theta e^{jk(x' \cos\phi \sin\theta + z' \cos\theta)} dx' dz' \quad (3.11c)$$

Where k is the free space wavenumber, r is the magnitude of the vector running from the origin to the point where the field is evaluated, ε is the permittivity of free space, r' is the magnitude of the vector running from the origin to any arbitrary point $(x', 0, z')$ on the

aperture surface, ψ is the angle between \mathbf{r} and \mathbf{r}' , and θ and ϕ are defined with respect to the coordinate system illustrated in Fig. 3.1. Only the ϕ component of the radiated field is considered here. While the r and θ components can be derived, it can be shown that they are negligible in the far field for the distributions considered here.

In order to proceed, the function $f(z)$ must be defined. For the remainder of the analysis, $f(z)$ will be chosen to be the following:

$$f(z) = \sin\left(\frac{\pi z}{W}\right) \quad (3.12)$$

The utility of this choice will become clear as the analysis is carried out. It should be noted that if the corresponding magnetic field is derived from the electric field distribution with this $f(z)$ via Faraday's Law, the magnetic wall boundary conditions will not be met at the cavity sidewalls. However, for the sake of argument, let us consider this distribution valid for now.

The integral in Eqn. 3.11c can now be carried out to obtain the final far zone electric field expression for the aperture. This expression will be split into two parts; E_1 , the portion of the E -field that arises from the classic $\text{TM}^{x_{010}}$ mode distribution, and E_2 , the portion of the E -field that arises from the modification that includes $f(z)$. They are as follows:¹

¹ Note these fields arise from a shifted coordinate system wherein the origin is placed in the center of the lower cavity surface. This means that the bounds of integration are from $-W/2$ to $W/2$ in z and 0 to h in x and $f(z)$ must be changed to $\cos(\pi z/W)$ to retain the same shape.

$$\mathbf{E}_1 = \hat{\phi} \frac{A_1 k \omega e^{-jk r} W \sin \theta}{4 \pi r} * X * \frac{\sin Y}{Y} \quad (3.13a)$$

$$\mathbf{E}_2 = \hat{\phi} \frac{2 A_2 k \omega e^{-jk r} W \sin \theta}{r [(k W \cos \theta)^2 - \pi^2]} * X * \cos Y \quad (3.13b)$$

$$X = -j \frac{e^{j k h \cos \varphi \sin \theta} - 1}{k \cos \varphi \sin \theta} \quad (3.13c)$$

$$Y = \frac{k W}{2} \cos \theta \quad (3.13d)$$

$$\mathbf{E}_{tot} = \mathbf{E}_1 + \mathbf{E}_2 \quad (3.13e)$$

To get the total E -field that results from two radiating apertures, the fields listed above must be multiplied by an array factor derived from the separation, magnitude and phase relationships between the equivalent magnetization currents on each radiating aperture. Given that the currents on the apertures have equal magnitude and are in-phase, the array factor is as follows [6]:

$$AF = 2 \cos \left(\frac{k L_{eff}}{2} \sin \theta \sin \varphi \right) \quad (3.14)$$

Where L_{eff} is the effective patch length due to fringing electric field effects at the patch edges. For the purposes of this thesis, the effective length correction may be neglected, but an expression for it may be found in Balanis 14.2.1 [6]. We now have

$$\mathbf{E}_{tot}^{2aperture} = \mathbf{E}_{tot} * AF \quad (3.15)$$

as the final far zone electric field radiated by two patch antenna apertures. It should be reiterated that the other two apertures do not radiate non-negligibly in the far field for the $TM^{x_{010}}$ mode and since $f(z)$ was chosen to be symmetric in amplitude and sign about the center of the radiation apertures, this property holds for the $TM^{x_{010}}$ mode distribution.

Next, the directivity of the enhanced gain patch will be examined with respect to the $TM^{x_{010}}$ mode excitation.

3.2.2.Enhanced Gain Patch Directivity

Thus far, it has not been shown how any of the analysis choices result in enhanced gain over the traditional patch antenna. This will be addressed by deriving the directivity of the $TM^{x_{010}}$ mode radiation distribution.

The directivity of an antenna is defined as the maximum value the antenna's gain takes with respect to the radiated power. It does not take loss effects into consideration. The expression for the directivity D and parameters related to it are presented as follows:

$$D = \frac{\langle |\mathbf{S}| \rangle_{max}}{P_{rad} / 4\pi r^2} \quad (3.16a)$$

$$\mathbf{S} = \mathbf{E} \times \mathbf{H} \quad (3.16b)$$

$$\langle |\mathbf{S}| \rangle = \frac{|\mathbf{E}|^2}{2\eta} \quad (3.16c)$$

$$\eta = \sqrt{\frac{\mu}{\epsilon}} \quad (3.16d)$$

$$P_{rad} = \oiint \langle \mathbf{S} \rangle \cdot d\mathbf{s} \quad (3.16e)$$

Here, $\langle |\mathbf{S}| \rangle$ is the time-averaged magnitude of the radiated field Poynting Vector, which represents the electromagnetic power density of the fields in W/m^2 , r is the radial distance from the antenna, η is the intrinsic impedance of the radiation medium, and P_{rad} is the total power radiated by the antenna, which is found by taking the surface integral of the time-averaged Poynting Vector over an arbitrary closed surface in the far field that encompasses the antenna. In this case, the most convenient surface to use is a sphere, allowing us to represent the radiated power as

$$P_{rad} = \int_0^{2\pi} \int_0^\pi \frac{|\mathbf{E}|^2}{2\eta} r^2 \sin\theta \, d\theta d\phi \quad (3.17)$$

While the fields radiated by the TM^x_{010} ' mode have been solved, the field amplitude coefficients A_1 and A_2 are still undefined. To remedy this, we will define a variable q as the ratio of A_2 to A_1 and compute the directivity as a function of this ratio, i.e.,

$$q = \frac{A_2}{A_1} \quad (3.18)$$

A direction of maximum radiation must also be defined. For normal patch antennas, the direction of maximum radiation is the direction where $\varphi=0$ and $\theta=\pi/2$. Since it is desired for the enhanced gain patch radiation pattern to mirror that of a traditional patch as much as possible (in all aspects except for the gain and beamwidth, of course), no other direction will be considered with respect to the directivity. To be more precise, then, the values to be computed will be the antenna gain (neglecting loss) in the direction of a normal patch's maximum gain, and while it may be true that the gain of the TM^x_{010} ' mode fields may be higher in a different direction for any given value of q , these situations are not desirable within the scope of this thesis and will thus be neglected.

Now that the groundwork has been completed, the directivity corresponding to the TM^x_{010} ' mode fields can be computed as a function of the ratio q . This is done using the expressions above and MATLAB numerical integration techniques. Below is a plot of the directivity in dB as a function of q .

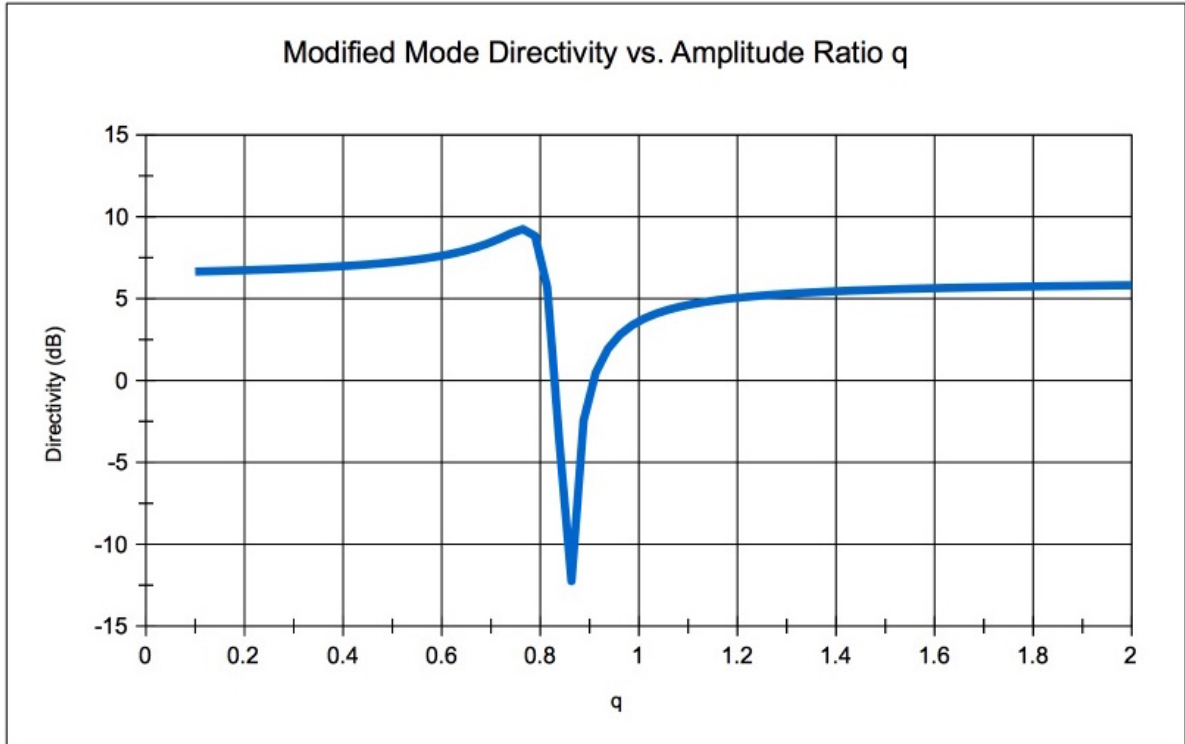


Fig. 3.2: Plot of the $TM_{x_{010}}$ mode directivity as a function of the amplitude ratio q . Design parameters for this case are as follows: $W=37.5\text{mm}$, $L=35\text{mm}$, $h=3.18\text{mm}$, $\epsilon_r=3.27$, and $f=2.4\text{GHz}$. Note design workflow is defined in chapter 5.

There are several important aspects to this plot. First of all, the directivity at very low q values (between approximately 0.1 and 0.4) represents the directivity of the standard $TM_{x_{010}}$ mode without modification, as A_2 in these cases is far smaller than A_1 , so the $f(z)$ modification to the modal profile has a negligible effect. This directivity is about 6.6 dB. However, starting around $q=0.5$, the directivity begins to rise until it peaks at approximately 9.2 dB for $q=0.76$ and then it falls sharply. What this means is that the $f(z)$ mode modification serves to raise the directivity in the direction being considered here for specific values of q , i.e., *our choice for $f(z)$ results in a modified mode that achieves clear significant directivity enhancement over the standard mode for these values of q* . It can also be seen that, if these values are passed, a destructive interference effect arises in the radiation direction being considered. The directivity increases again as the value of q con-

tinues to rise, but it never attains previous values. This behavior is not problematic, but it warrants mentioning.

While this result may seem promising, one crucial issue still has not been fully addressed; the fact that the $TM^{x_{010}}$ mode distribution presented technically is not valid under the patch cavity boundary conditions. This issue will be resolved in the following section.

3.3. Modified Mode Approximation Through Voltage Boundary Conditions

So far, it has been shown that a cavity mode can be designed in a way that results in an improved directivity over normal patch antennas. However, boundary conditions dictate what modes can and cannot be supported by the cavity. Again, the modified mode presented above is not a solution to the wave equation under the parameters we have set. Despite this, it will be shown that the modified mode distribution can be sufficiently approached, if not exactly achieved. How this is done is laid out below.

3.3.1. Cavity Mode Voltage Profile

The voltage profile of the modified mode with respect to the cavity upper and lower surfaces (i.e., the patch and the ground plane) may be easily derived as the following:

$$V = hE_x^{010'} \quad (3.19)$$

This is to say that the electric field distribution has a voltage distribution uniquely associated with it (since the E -field is purely x directed) that is represented through the equation above. This is significant because while it may not be possible to control the electric field directly through the cavity design, it may be possible to control it by manipulating voltages in and around the cavity. This is, in fact, the approach taken while implementing the enhanced gain patch. If a desired voltage distribution is defined, an excitation scheme

may be designed that results in this voltage distribution, and if such a scheme is established, the voltage values will be absolute to the point where the voltage profile may be seen as its own boundary condition. Unlike the cavity magnetic walls, this is a boundary condition whose nature can be controlled and the electric field on the aperture surfaces will result directly from it. By doing this, we would be somewhat forcing the electric field to take the shape we want by defining the voltage profile boundary condition. However, just because a theoretical voltage distribution results in enhanced gain, does not mean the cavity alone would be receptive of such a distribution. After all, the cavity wall boundary conditions still exist. There is a way around this, however, that will be detailed in the following section.

3.3.2. Multi-Pronged Feed Network Superposition

Recall that it was stated that the feed networks for the designs presented in this thesis play a role beyond simple excitation. This role is that they allow for the patterns afforded by the modified voltage distributions to be imitated without violating any boundary conditions. Refer to the figure below for an example antenna-feed network pair:

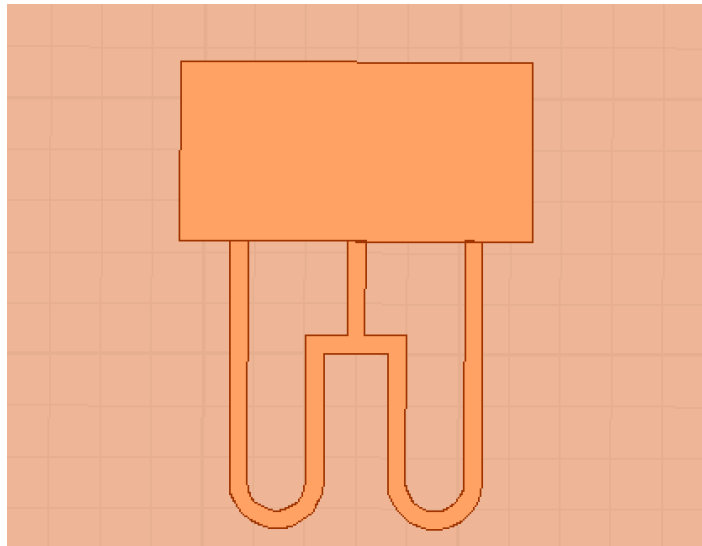


Fig. 3.3: Example enhanced gain structure topology where the feed lines are implemented in microstrip.

In the structure pictured above, the primary excitation for the entire circuit would be placed at the junction where all three feed lines connect (neglecting the matching network). Knowing this, it is clear that each antenna connection point will have a voltage that is different from each adjacent feed point, i.e., the voltages at the outer feed points will have a differing voltage from that of the mid feed point. Normally, this would be at odds with the patch's dominant mode voltage distribution. However, the feed network connections on the feed plane provide the leeway necessary for the patterns of the modified voltage distributions to be obtained. To put another way, while the patch itself cannot support an arbitrary voltage distribution natively, the patch and the specially designed feed network above can be combined to form the enhanced gain pattern predicted by the theory.² This is because, given the patch impedance characteristics on the feed plane, the voltages themselves may be thought of as their own boundary conditions, so if the network is designed correctly, the voltage distribution can supersede the magnetic wall boundary condition and modified modes may be excited. How this is done exactly will be detailed in the following chapter.

Further, as will be demonstrated in the design process, the network may be designed as if the voltage distribution is being supported by the patch and the patch alone, i.e., the feed network lines may be treated like normal transmission lines connected to conventional loads during most of the design process. This is not to say that a final design can be fully created using only theory (at least within the scope of this thesis), but the design methods to be discussed in later chapters provide a very reasonable starting point and empirical tweaking is minimal.

² Even patterns with the topside gain null illustrated in Fig. 3.2 may be created using this method.

3.4. Conclusions

In this chapter, the theory behind the enhanced gain patch formulation was defined. It can be seen that theoretical gain enhancement can be achieved if a custom modal distribution is created in the patch cavity. It was also claimed that the way to create this distribution is through applying a specialized feed network to imitate the desired voltage distributions. Let it be noted that while it is possible that another choice of $f(z)$ would yield similar results, such cases will not be considered in this thesis, as the chosen $f(z)$ serves our purposes. In the next chapter, a detailed analysis of the feed network design process will be carried out.

4. ENHANCED GAIN PATCH ANTENNA FEED DESIGN

This chapter will focus on developing the design techniques for obtaining the desired voltage boundary conditions on the enhanced gain patch. It will begin by defining the general feed network structure, after which the methods for finding feed network parameters will be discussed. Finally, the integration of an impedance matching network will be examined, concluding the feed network discussion. Again, the methods described here will assume that the feed network does not radiate and that voltage distributions are created directly on the patch apertures.

4.1. Tuned Transmission Line Network Formulation

As stated in chapter 3, multiple feed points must be established in order to realize a particular voltage distribution. To accomplish this, three distinct “ports” will be defined on the edge of one of the radiating apertures, and three microstrip transmission lines will be connected to those ports and to each other at a separate junction away from the patch, not unlike a corporate feed. This ensures that the antenna will eventually need only one feed source. Fig. 4.1 re-illustrates this concept.

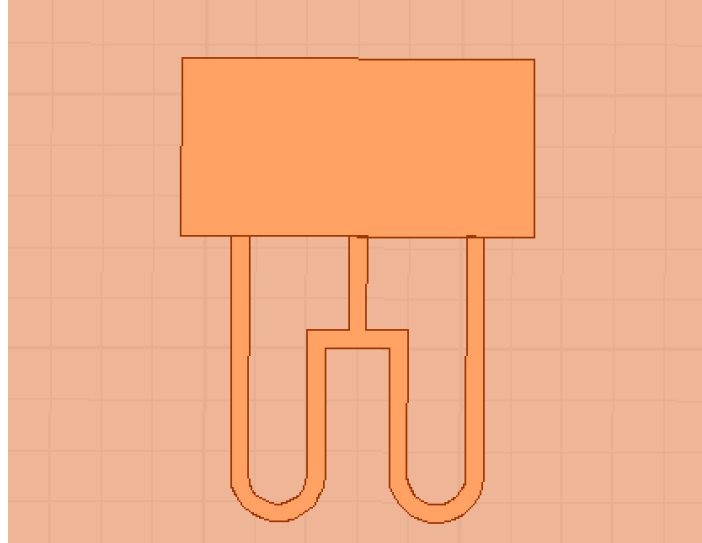


Fig. 4.1: General feed network design (without a matching network). Three microstrip lines are connected to three points on the patch edge and then they are connected to each other.

The chosen separation between the patch center feed point and the side feed points for the formulation presented here is $W/3$, although other separations could conceivably be effective and the design methods do not change based on this parameter.

Clearly, there are two parameters that must be defined for the network; line lengths and characteristic impedances. In order to find the parameters that will result in the desired voltage distribution, Z -matrix and transmission line theory must be invoked. This will be done in the following sections.

4.1.1. Z -Matrix Analysis and Port Parameter Definitions

By defining three feed points on the patch, we are essentially creating a 3-port network, and thus, we may use Z -matrix analysis to examine it. The Z -matrix for a 3-port network is defined via the following equation [7]:

$$[\mathbf{V}] = [\mathbf{Z}][\mathbf{I}] \quad (4.1a)$$

$$\begin{bmatrix} V_1 \\ V_2 \\ V_3 \end{bmatrix} = \begin{bmatrix} Z_{11} & Z_{12} & Z_{13} \\ Z_{21} & Z_{22} & Z_{23} \\ Z_{31} & Z_{32} & Z_{33} \end{bmatrix} \begin{bmatrix} I_1 \\ I_2 \\ I_3 \end{bmatrix} \quad (4.1b)$$

Where V_i is the total voltage presented to port i , I_i is the total current presented to port i , and Z_{ij} is the impedance parameter that describes the voltage present at port i due to a current present at port j when the currents at all ports other than port j are 0. Once the feed points are defined, the corresponding Z parameters may be computed through computer electromagnetic simulation.³

Using the expressions above, we may define the driving point impedances (DPIs) at each port, which are the total impedances seen at each port when all ports are active.

These expressions are as follows:

$$Z_{1d} = \frac{V_1}{I_1} = Z_{11} + Z_{12} \frac{I_2}{I_1} + Z_{13} \frac{I_3}{I_1} \quad (4.2a)$$

$$Z_{2d} = \frac{V_2}{I_2} = Z_{21} \frac{I_1}{I_2} + Z_{22} + Z_{23} \frac{I_3}{I_2} \quad (4.2b)$$

$$Z_{3d} = \frac{V_3}{I_3} = Z_{31} \frac{I_1}{I_3} + Z_{32} \frac{I_2}{I_3} + Z_{33} \quad (4.2c)$$

³ All electromagnetic simulations in this thesis were carried out using ANSYS HFSS.

Where Z_{id} is the driving point impedance at port i . Right away, it should be noted that the voltage and impedance seen at any one port depends on the current excitations on all of them. The only way to control each port's voltage independently of the others would be to isolate the ports electrically and electromagnetically, which is impossible in the cases being considered here. However, as seen above, the driving point impedances of each port depends not simply on the port current values, but on the port current *ratios*. This means that if certain current ratios are desired, the driving point impedances corresponding to these current ratios may be found.

It has been established that a certain voltage distribution is desired at the feed plane, but this distribution need not take a particular amplitude. The total voltage profile may be multiplied by any arbitrary constant without changing the gain characteristics of the corresponding electric field. Because of this, we may design the feed network with respect to the normalized voltage distribution. Given how the modified mode was defined in chapter 3, the voltage on the center feed will have a higher amplitude than the voltage on the outer feeds; these "side" voltages (which will from now on be denoted as V_{side}) will be defined to have a voltage of 1 V . The voltage of the middle feed (V_{mid}) will thus be defined by the following equation:

$$V_{mid} = \frac{1+q}{1+q/2} \quad (4.3)$$

where q is the same as in Eqn. 3.18. This equation is easily derived from Eqn. 7, Eqn. 12, and Eqn. 19 evaluated at $y=0$ with the side voltages located at $W/3$ away from the center feed point (which is located at $z=0$).

Once the desired value of q is found via the directivity analysis in 3.2.3, the side and middle voltages may be defined. From there, the corresponding currents may be found via the following relation:

$$[\mathbf{Z}]^{-1}[\mathbf{V}] = [\mathbf{I}] \quad (4.4)$$

This equation is obtained simply by inverting the Z-matrix in Eqn. 4.1a. With this information, the DPIs that will occur with the desired voltage distribution may be computed. These values are essential for the analysis to come.

Now that all the initial parameters have been set, we may define a method for defining the feed network characteristics. This will be done in the following section.

4.1.2. Voltage Ratio Transformation Analysis and Locked DPI Assumption

For the following derivations, let

$$V_{side} = V_1 = V_3 \quad (4.5a)$$

$$V_{mid} = V_2 \quad (4.5b)$$

This is to say that the side ports are equivalent to ports 1 and 3 (which are equivalent to each other given the symmetry) and the center port is equivalent to port 2.

Because all the feed lines connect in a central location, they all share the same voltage at that point. We may use this fact, along with the general transmission line voltage wave solution to derive the following port voltage relationship:

$$\frac{V_2}{V_1} = \frac{(1 + \Gamma_2)(e^{j\theta_1} + \Gamma_1 e^{-j\theta_1})}{(1 + \Gamma_1)(e^{j\theta_2} + \Gamma_2 e^{-j\theta_2})} \quad (4.6a)$$

$$\Gamma_1 = \frac{Z_{1d} - Z_{o1}}{Z_{1d} + Z_{o1}} \quad (4.6b)$$

$$\Gamma_2 = \frac{Z_{2d} - Z_{o2}}{Z_{2d} + Z_{o2}} \quad (4.6c)$$

Where Γ_i is the reflection coefficient on the line connected to port i , θ_i is the electrical length of the line connected to port i in radians, Z_{oi} is the characteristic impedance of the line connected to port i , and the Z_{id} are the port DPIs as normal. This means that if the transmission line parameters are correctly chosen, the following equation must hold:

$$\frac{1 + q}{1 + q/2} = \frac{(1 + \Gamma_2)(e^{j\theta_1} + \Gamma_1 e^{-j\theta_1})}{(1 + \Gamma_1)(e^{j\theta_2} + \Gamma_2 e^{-j\theta_2})} \quad (4.7)$$

This equation contains at least four unknowns (the transmission line electrical lengths and characteristic impedances), so it will be solved through a numerical guess-and-check iterative algorithm implemented in MATLAB. There is an issue, however, in that the Γ values cannot be used in such an algorithm as they are now. This because they depend on the DPIs, which in turn depend on the realized port current ratios, which are unknown for any arbitrary set of transmission line parameters because, in a seemingly paradoxical manner, given the available information, *it is impossible to solve for the current ratios without already knowing what they are*. To state this another way, the voltage and current

transformations that allow us to obtain expressions for the voltages and currents on the patch edge require prior knowledge of these voltages and currents in order to be evaluated, leading to a circular dependence.

There is a way around this, fortunately, that hinges on an assumption called the “Locked DPI Assumption”. While it may not be known what the port DPIs are for any given set of transmission line parameters, it is known what the DPIs would be if the desired voltage distribution were to be realized, i.e., we can solve for the DPI values that are linked to the q value of the distribution we wish to implement. Under the Locked DPI Assumption, the DPIs take these would-be values regardless of the other equation parameters, i.e., while the other equation parameters are iterated in the algorithm, the DPIs will be “locked” at values corresponding to the desired port voltage/current ratios.

This formulation is effective because of one fundamental truth; *if Eqn. 4.7 holds for any arbitrary set of transmission line parameters under the Locked DPI Assumption, then this assumption also holds for this set and a valid solution has been found.* To put it more generally, if an assumption is made in a circular problem such as the one presented here, and then an analysis is carried out that yields a result that must be true under the assumption, then the assumption is also true. In terms of the guess-and-check algorithm, this means that we may define the RHS of Eqn. 4.7 in terms of the locked DPIs and transmission line parameter “guesses”, and if a guess results in the desired voltage ratio, then a valid solution has been reached despite the fact that we have made an assumption about the DPIs. In the next section, the details of the algorithm will be highlighted.

4.1.3. Transmission Line Parameter Definition

To determine a solution for Eqn. 4.6a, four parameters (the transmission line electrical lengths and characteristic impedances) must be iterated within a range specified judiciously by the designer. For instance, for microstrip transmission lines, a rule of thumb is to only consider lines with a characteristic impedance between 25 and 150 Ω , otherwise,

the line implementations will become prohibitively wide or narrow. Further, since the lines are connected to the same antenna, the lower bound for the characteristic impedance should be significantly more than 25Ω in order to prevent the formulation presented here from breaking down due to unacceptably large coupling effects. For this reason, the lower bound for the impedances to be checked by the algorithm should be set between 50 and 100 Ω . As for the electrical lengths, it is desirable for the lines to be as short as possible, so a range from 0 to $\pi/2$ radians should be used initially, and the upper bound should be increased only if a satisfactory solution cannot be found within this range.

Once the parameter ranges are defined, the algorithm, starting with initial parameters, evaluates the RHS of Eqn. 4.6a (using the locked DPIs as well) and determines how close the resulting voltage ratio is to the desired value. If the computed value is within a user-defined tolerance, the algorithm outputs the set of transmission line parameters that results in the accepted value and the algorithm ends. Otherwise, the parameters are iterated using a nested loop scheme and the process restarts. If no parameter set that gives a value within the tolerance is found, the algorithm outputs the set that results in the closest voltage ratio to the desired value that can be found within the specified parameter ranges. It should be noted that multiple solutions within the tolerance may be found within a certain range and the algorithm only outputs the first one it finds. Therefore, one may experiment with the parameter range definition to get a result with more desirable characteristics, such as a shorter line or a smaller characteristic impedance. In this sense, the “solution” to Eqn. 4.6a is not unique, and multiple design variations are possible. The full MATLAB code that accomplishes this process is presented in the appendix.

Using this set of transmission line parameters, a feed network circuit may be designed in a full-wave computer simulation program such as ANSYS HFSS in order to observe the radiation characteristics of the patch and feed network combination. It should be noted that the feed network derived from the algorithm will often not result in the exact radiation characteristics of the desired voltage distribution. This is because the feed net-

work itself will load the circuit, altering impedance parameters and causing deviations from the theory. This means that, using the simulation software, the feed network must be tweaked in order to get the desired response. However, the modifications that must be made are not major (they simply involve changing the line lengths slightly until the correct pattern is achieved), so the algorithm presents an effective starting point for the design. Also note that when line lengths are defined, any multiple of a half wavelength may be added to the computed values without changing the voltage distribution on the antenna. This is useful logistically as it allows us to make the side excitation feeds long enough to connect to the line junction.

The algorithm outlined above computes the parameters for the feed network that gives a desired voltage distribution, but it does not address the impedance looking into feed line junction, which is where the source would be connected. This will be addressed in the following section.

4.2 Matching Network Design

Since the feed network must be modified to achieve the desired radiation characteristics, much of the matching network design is empirical. There is, however, an effective standard procedure that will be developed here, assuming the network is to be matched to a standard impedance like 50Ω . The matching networks designed for the prototypes to be presented in this thesis are all implemented as two-stage transmission line circuits defined with respect to the impedance seen at the feed line junction.⁴ These stages are outlined below:

⁴ Note the MATLAB code also stipulates what junction input impedances are acceptable.

4.2.1. Stage 1: High Impedance Line Section

Once the impedance of the feed line junction is extracted from simulation software, a high-impedance line (typically between 100 and 150 Ω) is connected to the feed junction. The purpose of this line is to transform the junction impedance until it is resonant and to extend the projected source feed point toward the substrate edge so that the circuit may be fed via an edge mount PCB connector.

Referring to Fig. 4.1, it can be seen that the side feed lines extend past the feed line junction and wrap around to make their way back to it. This was done because the derived line lengths for the side feeds were too short for these lines to make it to the transmission line junction, so an extension (whose length was a multiple of a half wavelength) was added to each side line. As such, the first matching network stage will run parallel to these lines. This is one reason why higher impedance lines are used for stage 1, as they lessen potential coupling effects between the stage and adjacent lines. Once a purely real, sufficiently high impedance is realized with the stage 1 line, stage 2 may be implemented.

4.2.2. Stage 2: Quarter-Wave Transformer

The second stage is a standard quarter-wave transformer used to scale the resonant impedance created by stage 1 to the desired value. While its width is not subject to the same constraints as the stage 1 line, stage 1 should still be designed such that the required transformer width is not too large or small. The impedance of the quarter-wave transformer can be easily found with the well documented relation:

$$Z_{trans} = \sqrt{Z_o Z_{res}} \quad (4.8)$$

Where Z_{trans} is the transformer characteristic impedance, Z_{res} is the resonant impedance seen looking into stage 1, and Z_o is the source impedance.

Fig. 4.2 illustrates the full enhanced gain patch circuit.

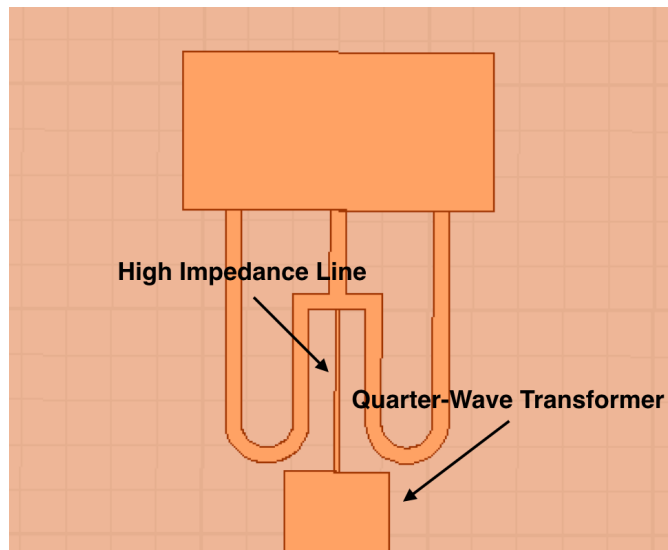


Fig. 4.2: Complete enhanced gain patch circuit with impedance matching section

4.3. Conclusions

In this chapter, it has been shown how the feed network needed to achieve enhanced gain is designed. The theory and numerical analysis behind the required transmission line circuits was also defined and discussed, culminating in methods to implement the enhanced gain patch. This completes the foundational development for the design process. In the next chapter, a full summary of the design workflow from start to finish will be detailed.

5. ENHANCED GAIN PATCH DESIGN WORKFLOW

In this chapter, a complete design workflow will be defined to allow any designer to utilize the methods developed in this thesis. The design process requires a numerical computing platform (such as MATLAB) as well as a full-wave EM simulation software package (such as ANSYS HFSS). The chapter will be structured in a step-by-step format that will detail all crucial design steps.

5.1. Step 1: Substrate and Patch Dimension Definition

The chosen substrate for the patch should have mid to high permittivity and should be thin enough to mitigate unwanted radiation effects in the feed network. For instance, the substrate for the prototypes in this thesis has a thickness of 3.18mm and a relative permittivity of 3.27 and these parameters work sufficiently well, as we shall see, although the thickness for a substrate with this permittivity should not be increased. With this in mind, the substrate choice should be left up to the designer's discretion as with any other application. As for the board dimensions, it is recommended that the board be around two substrate wavelengths long and wide. The designer should expect the full circuit to be at least 1.5 wavelengths long so the board must be able to accommodate this. Other board dimensions are theoretically possible, although the patch's proximity to the board edges affects both the pattern and impedance values, so changing the board dimensions during the design process would require the designer to redo steps 3 and on.

Patch dimensions that are appropriate for the desired resonant frequency must also be chosen. In particular, W and L must be defined. L must be approximately a half wavelength as is the case with traditional patches, but W is more flexible since the resonant frequency of the target mode only depends on L . There are tradeoffs to consider when

choosing W , however, that should be taken into account, some of which will come to light in following chapters. The prototypes to be presented all have widths between approximately $.5\lambda$ and 1.23λ where λ is defined with respect to the effective permittivity of the substrate when considering a microstrip line (as oppose to the free space wavelength). L is locked at 35mm for these prototypes (note it is slightly shorter than a half wavelength to account for fringing field length extension).

5.2.Step 2: Voltage Profile Definition

Once the patch dimensions are chosen, the desired modal amplitude coefficient ratio may be defined. This can be done graphically by generating a plot similar to Fig. 3.2 (note the MATLAB code that accomplishes this is given in the appendix). After the relevant q value is extracted, Eqn. 4.3 may be used to find V_{mid} when V_{side} is 1 V.

5.3.Step 3: Z-Matrix Extraction

In this step, the Z-parameters for the three feed ports on the patch edge are computed using an EM simulation software. For this thesis, step 3 was completed in HFSS by defining three lumped port boundaries and extracting the resulting Z-matrix from the simulation. An example of this port definition is pictured below in Fig. 5.1.

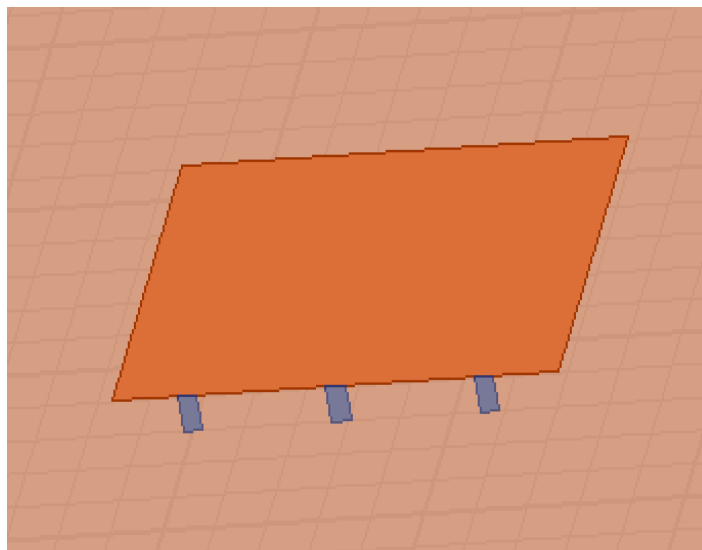


Fig. 5.1: Example Z-parameter extraction scheme

Note that the width of these lumped port boundaries correspond to the maximum desired microstrip feed width. For instance, in the example above, the minimum characteristic impedance considered in the design process was 100Ω , which corresponds to a width of 1.85 mm. Note that this is a rough guideline and need not be exact. If, for example, the minimum considered characteristic impedance is changed by the designer after this step is completed, the step does not explicitly need to be revisited. All that is really required of the ports is sufficient spatial isolation.

5.4.Step 4: Initial Feed Network Definition

This step defines a starting point for the feed network implementation using the Z-parameters and voltage ratios. These parameters are entered into a code like the MATLAB script discussed in section 4.1.3 to compute the initial set of transmission line lengths and characteristic impedances that will approximate the desired voltage distribution. Again, note that any integer multiple of a half wavelength may be added to these computed lengths without changing the distribution on the patch.

5.5.Step 5: Initial Feed Network Implementation and Tweaking

After the transmission line parameters are obtained, the initial feed network is modeled in an EM simulation software. At this point, the circuit looks like the one picture in Fig. 4.1. For the reader's convenience, it is pictured again below.

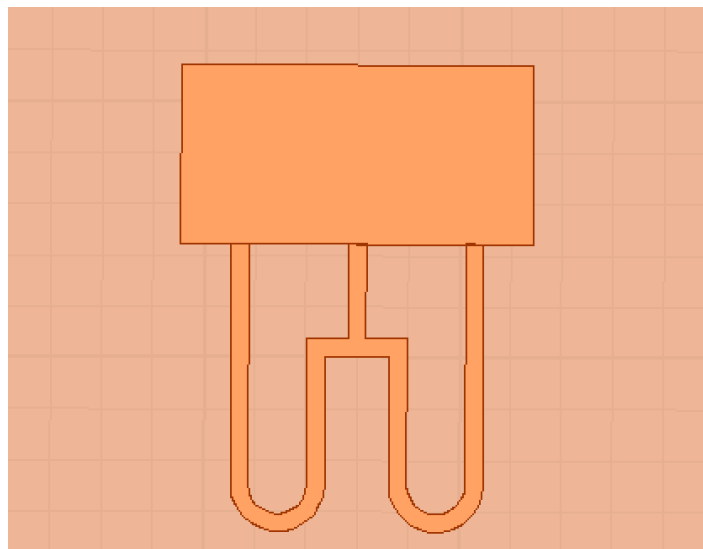


Fig. 5.2: Initial feed network

An excitation is then placed at the feed line junction and the circuit is simulated to observe the directivity. Generally, the observed value will not reflect the desired solution after the first simulation, so the feed lines must be optimized using a trial-and-error approach (due to the deviations from the theory resulting from the radiation condition). This does not negate the usefulness of steps 1-4 however, as it has been observed that the feed network need not be drastically changed to excite a satisfactory distribution. It was found that lengthening or shortening the line lengths in 5mm increments (either all together or by changing the side line lengths independently of the middle one) and observing the trends in the resulting directivity pattern was sufficient to create the desired voltage profile, although changing the characteristic impedances also has an affect, albeit a smaller one.

It is also important to track the input impedance at the junction to make sure no extreme values are reached. No particular impedance value is required, but the reactance at the junction should never exceed the resistance by more than one order of magnitude. Additionally, the resistance should be $\gg 1$. Not adhering to these conditions would make designing a suitable matching network far less viable. Further, the length of the side feed line wraparound (the portion of the line that extends past the junction) should dictate the ideal relative position of the junction impedance on a Smith chart for a reference impedance of about 100Ω and up. This is because the first stage of the matching network must be at least as long as this wraparound, so it is desirable for the length required to achieve resonance to also equal the wraparound length. Fortunately, a sufficient directivity pattern can generally be realized while keeping these impedance conditions in mind.

5.6.Step 6: Matching Network Design

Designing the first stage of the network may be done empirically, graphically or numerically. The empirical approach involves simply extending a high impedance line (no exact value is required; it is up to the designer) from the junction and observing the impedance at the other end, then iterating the line until resonance is reached. Graphically,

this can be done by using a Smith Chart to determine the necessary line length needed for resonance with a given line characteristic impedance. Finally, a code can be written using transmission line theory to compute the desired line length using a guess-and-check iterative algorithm similar to that used for the initial feed network definition.

All the prototype matching networks in this thesis were designed using the empirical method, and this is recommended since coupling between the first stage of the matching network and the side feed lines has a non-negligible effect on the input impedance of this stage (although it does not compromise the ability to obtain resonance). After stage 1 is completed, a simple quarter-wave transformer is applied using Eqn. 4.8, after which the design is completed.

It is worth noting that, if the empirical method is chosen and the board dimensions are finite, the patch should not be moved any closer or farther away from the board edges during the matching network design process. This is because moving the patch around on the board changes the mutual impedances on the ports and thus detunes the patch, leading to unexpected impedance effects.

Finally, if the junction impedance value does not lead to a favorable network (if the stage 1 line extends significantly passed the wraparound for example), then step 5 should be revisited and the circuit should be tuned to lead to better impedance values while retaining enhanced gain properties.

5.7.Conclusions

In this chapter, step-by-step instructions for designing an enhanced gain patch from beginning to end were presented, providing a full design workflow for the structure. In the next chapter, four experimentally verified prototypes that were fabricated for this thesis project will be presented and discussed, demonstrating both the efficacy and the tradeoffs of the enhanced gain patch antenna.

6. PROTOTYPE DESIGNS AND RESULTS

This chapter will be devoted to presenting and discussing four prototype structures that were designed using the formulations in previous chapters. These structures were fabricated and measured to confirm the efficacy of the techniques discussed in this thesis. The chapter will begin by illustrating the dimensions of each design, followed by the presentation of the radiation pattern and return loss results. These results will also be compared to those of an unmodified patch antenna to be used as a reference. Finally, the tradeoffs of the prototypes will be discussed.

6.1. Prototype Dimensions

Each prototype was optimized for operation at ~ 2.4 GHz and was fabricated on a 150mm x 150mm, 3.18mm thick Rogers TMM 3 substrate with a relative permittivity of 3.27. Below is a figure illustrating the general dimensional variables of each prototype, followed by a table giving the specific values for each individual structure in millimeters. They are as follows:

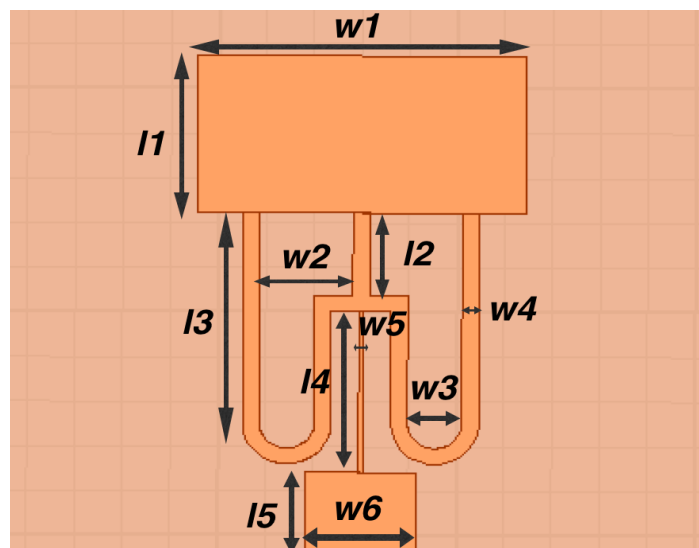


Fig. 6.1: General patch dimension diagram

Table 6.1: Patch dimension values. All values are in mm.

*upper half of the matching stage is 5mm and lower half is 1mm.

Prototype Number	<i>w1</i>	<i>w2</i>	<i>w3</i>	<i>w4</i>	<i>w5</i>	<i>w6</i>	<i>l1</i>	<i>l2</i>	<i>l3</i>	<i>l4</i>	<i>l5</i>
1	93.75	31.25	19.75	3.5	5, 1*	22	35	28	38	36	20
2	69	23	11.5	3.5	1	23	35	22	47	36	20
3	42.74	14.25	4.39	1.85	1	20	35	28	58	33	21
4	37.5	12.5	2.65	1.85	1	23	35	30	60	32	20

The reference patch design is pictured below:

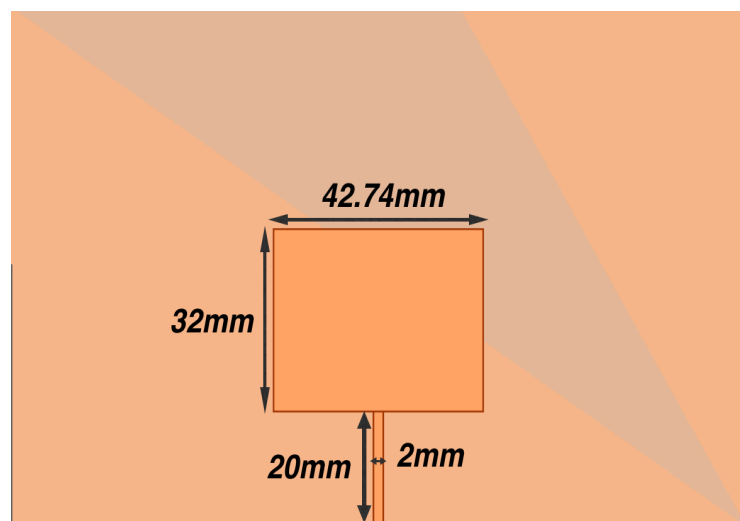


Fig. 6.2: Reference Patch Design

It should be noted that these designs are not unique, i.e., an enhanced gain pattern can be obtained using alternate dimensions. These dimensions, however, were found to give the desired results.

6.2.Measurement Results

In this section, the radiation pattern, return loss, and bandwidth results for the prototypes and the reference patch will be presented. They are given in the following subsections. All pattern measurements were taken using a standard cubicle anechoic chamber and a 2-port network analyzer. Note that only relative gain patterns were able to be taken, and all absolute gain values are given with respect to the reference patch instead of an isotropic radiator. In addition, each pattern has two sidelobes associated with it, as will be seen. The lobe in the positive y direction will be labeled the “front lobe” with its own “front lobe level” (FLL) and the lobe in the negative y direction will be labeled as the “back lobe” with its own “back lobe level” (BLL).

6.2.1.Prototype 1 Results

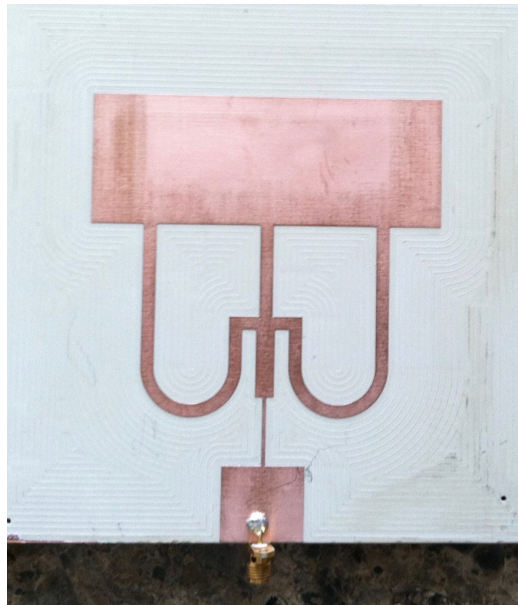


Fig. 6.3: Prototype #1 Implementation

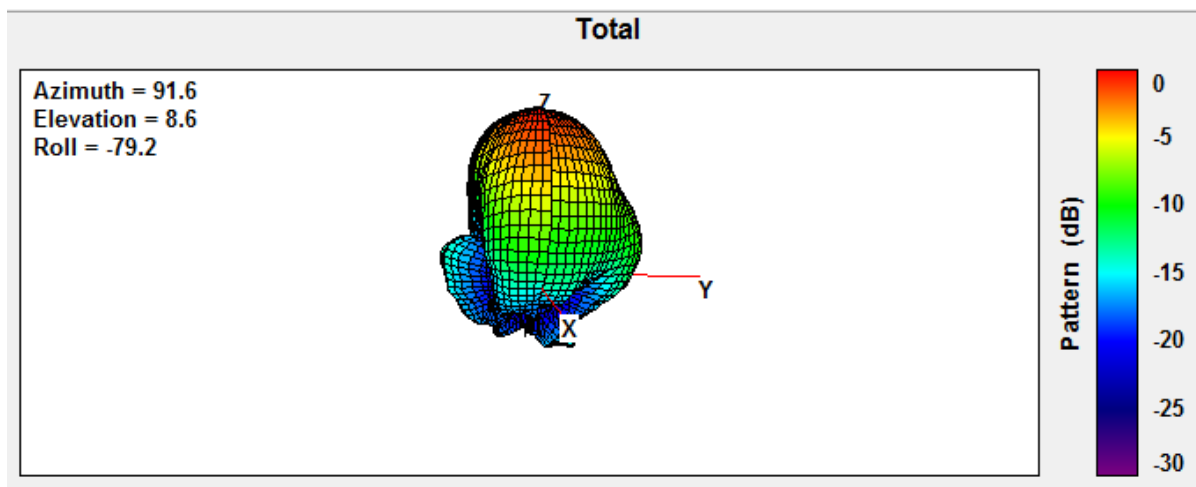


Fig. 6.4: Prototype #1 3-D Pattern

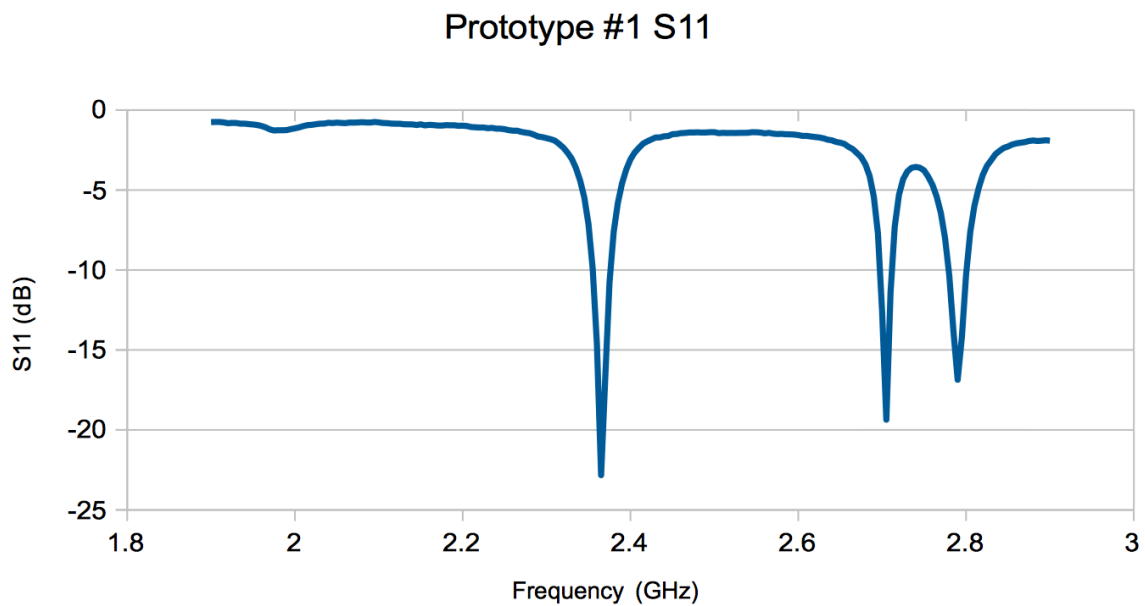


Fig. 6.5: Prototype #1 Return Loss

6.2.2. Prototype 2 Results

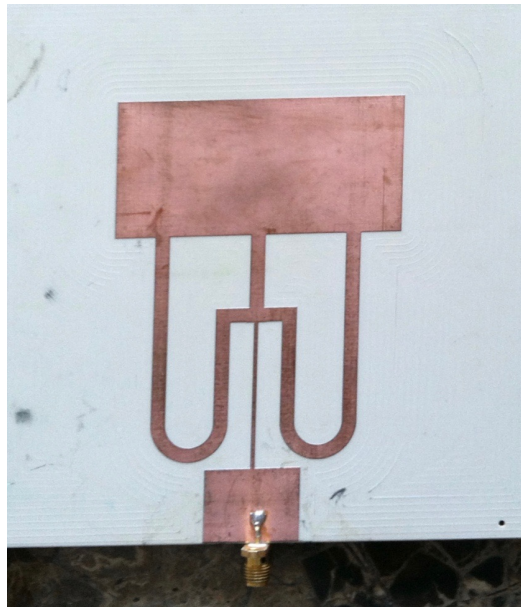


Fig. 6.6: Prototype #2 Implementation

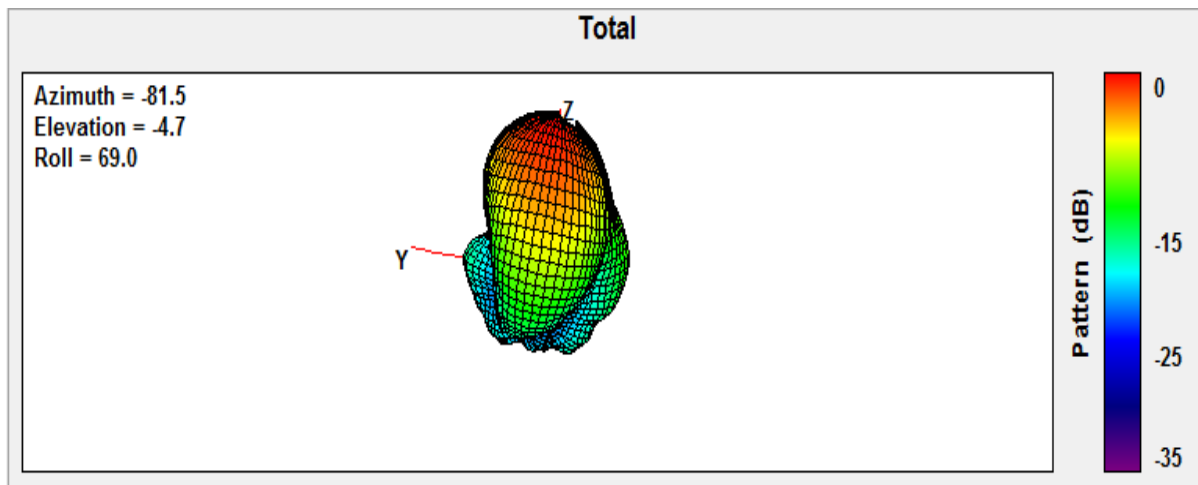


Fig. 6.7: Prototype #2 3-D Pattern

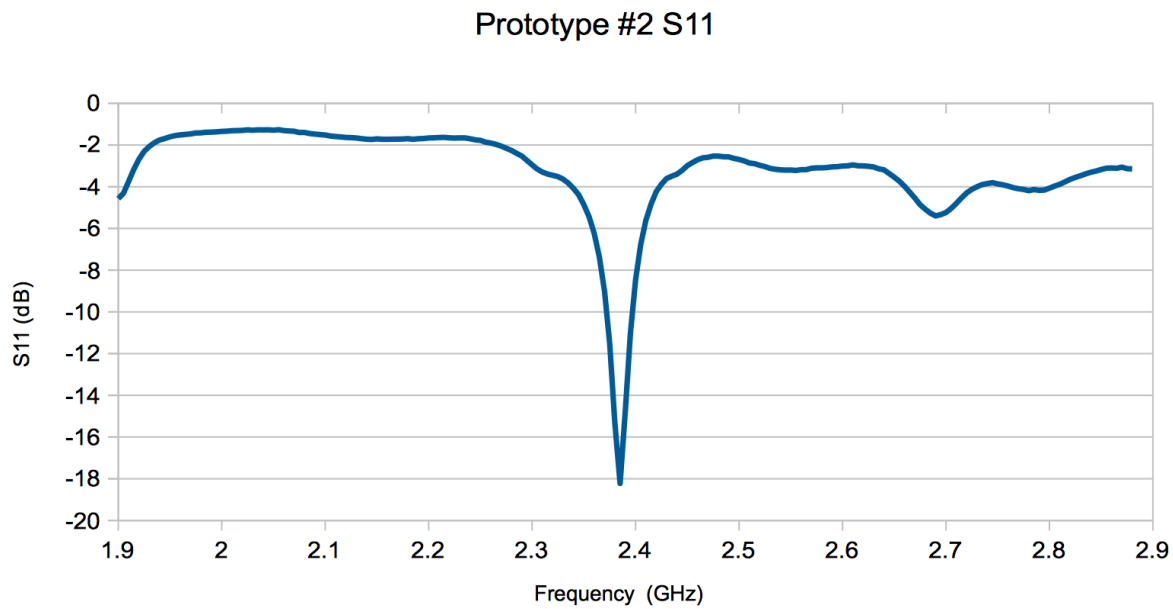


Fig. 6.8: Prototype #2 Return Loss

6.2.3. Prototype 3 Results

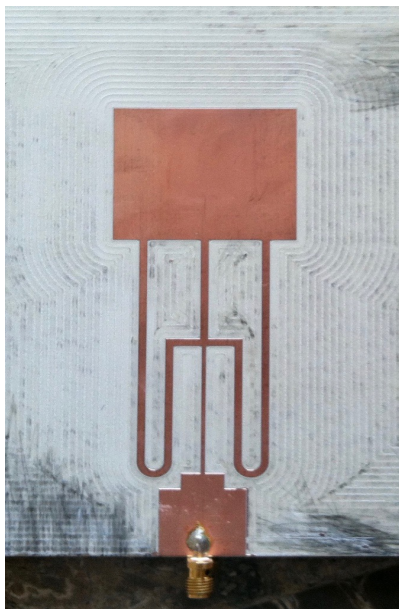


Fig. 6.9: Prototype #3 Implementation

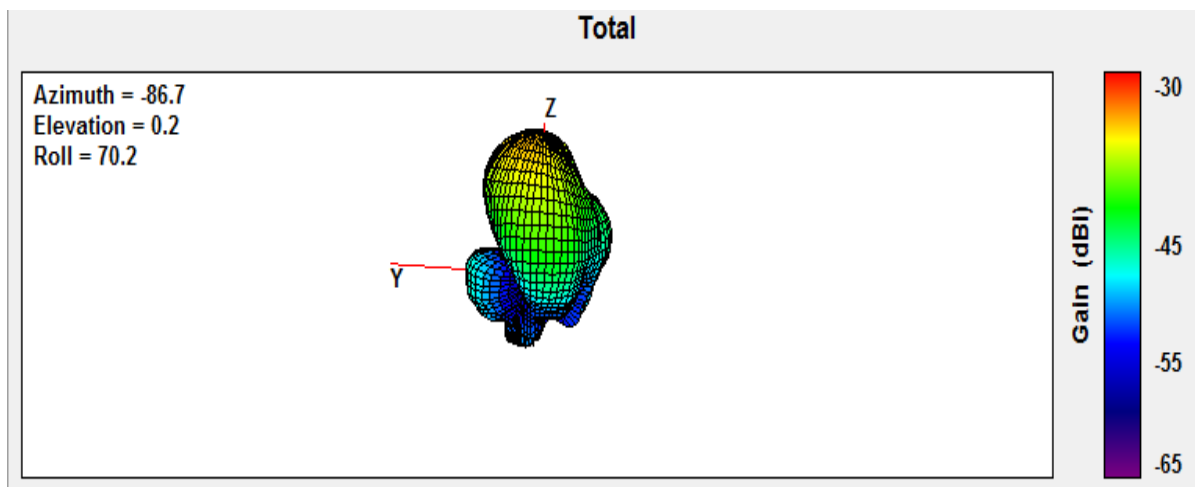
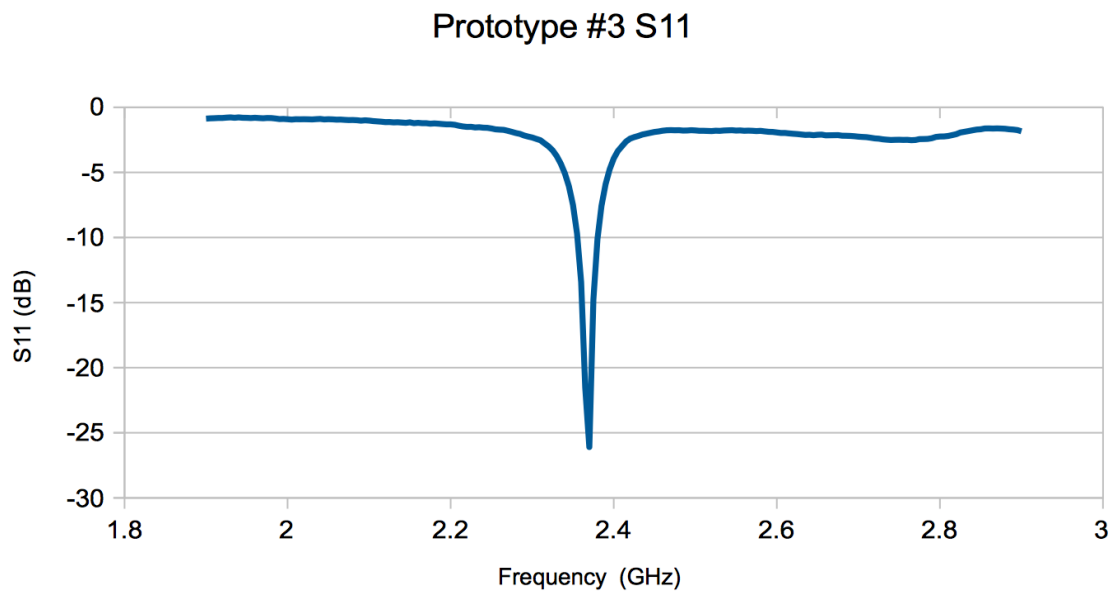


Fig. 6.10: Prototype #3 3-D Pattern



6.2.4. Prototype 4 Results

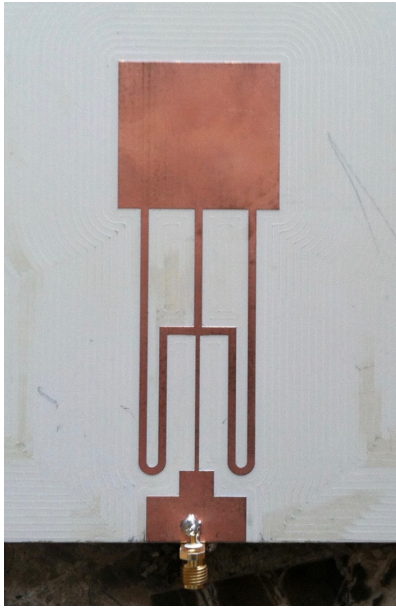


Fig. 6.12: Prototype #4 Implementation

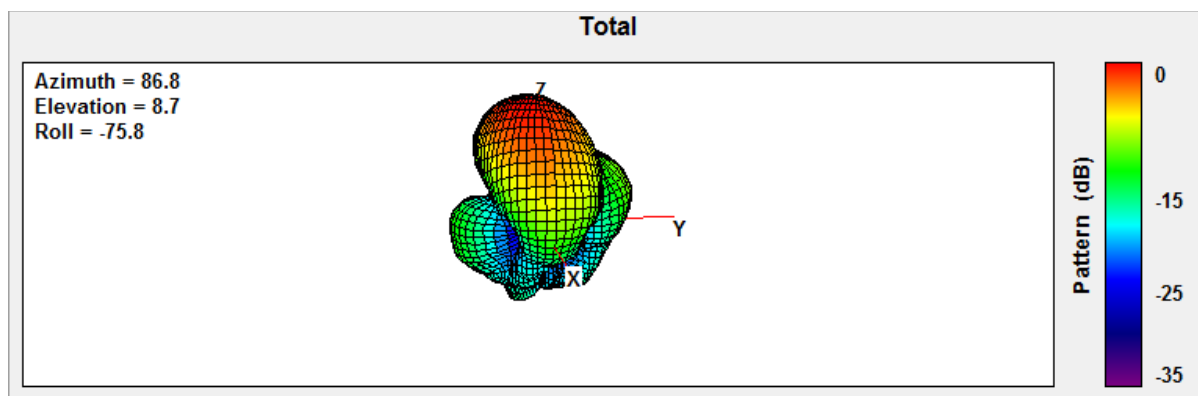


Fig. 6.13: Prototype #4 3-D Pattern

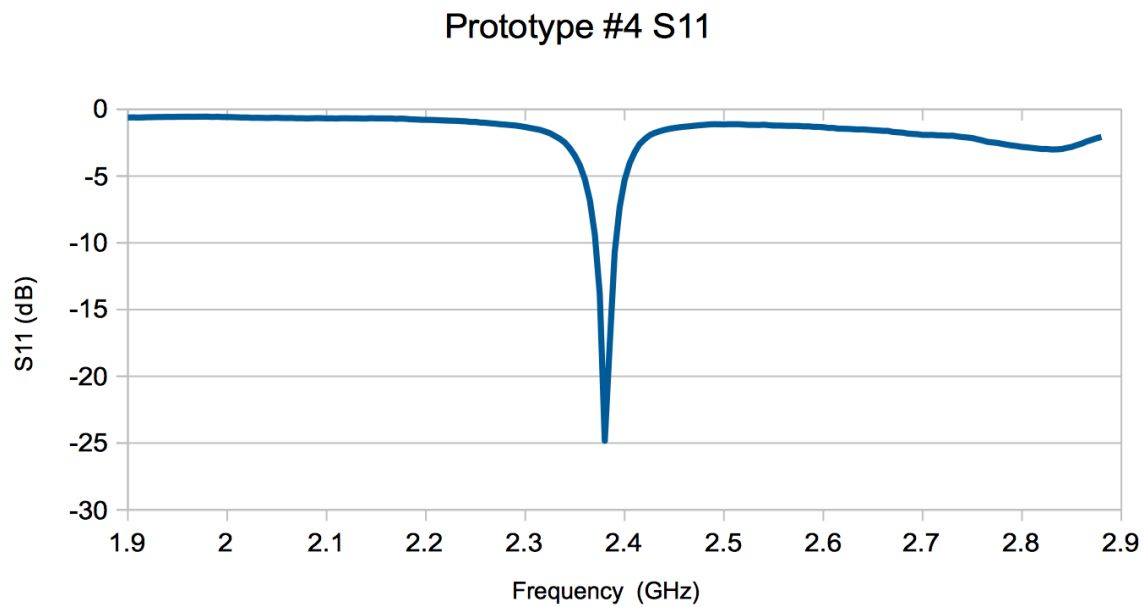


Fig. 6.14: Prototype #4 Return Loss

6.2.5. Reference Patch Comparison and Additional Results

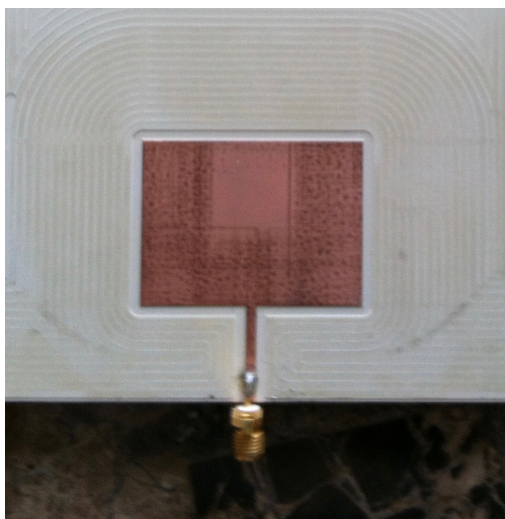


Fig. 6.15: Reference Patch Implementation

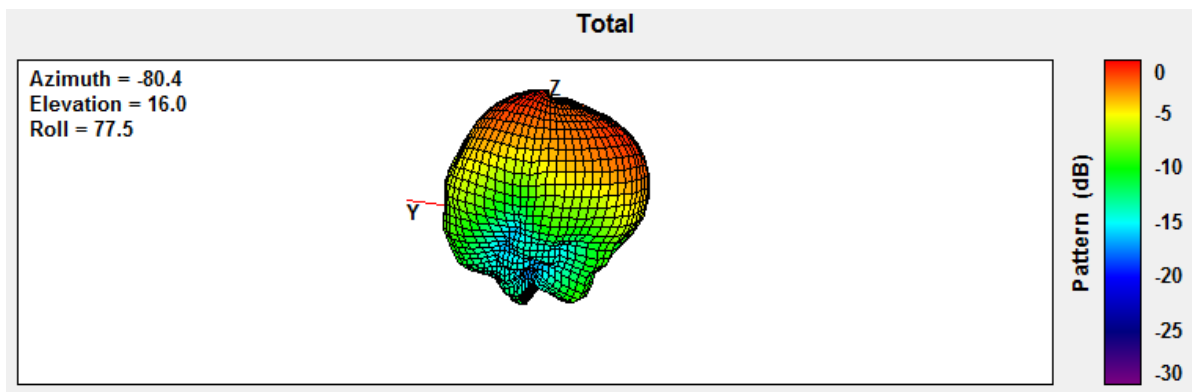


Fig. 6.16: Reference Patch 3-D Pattern

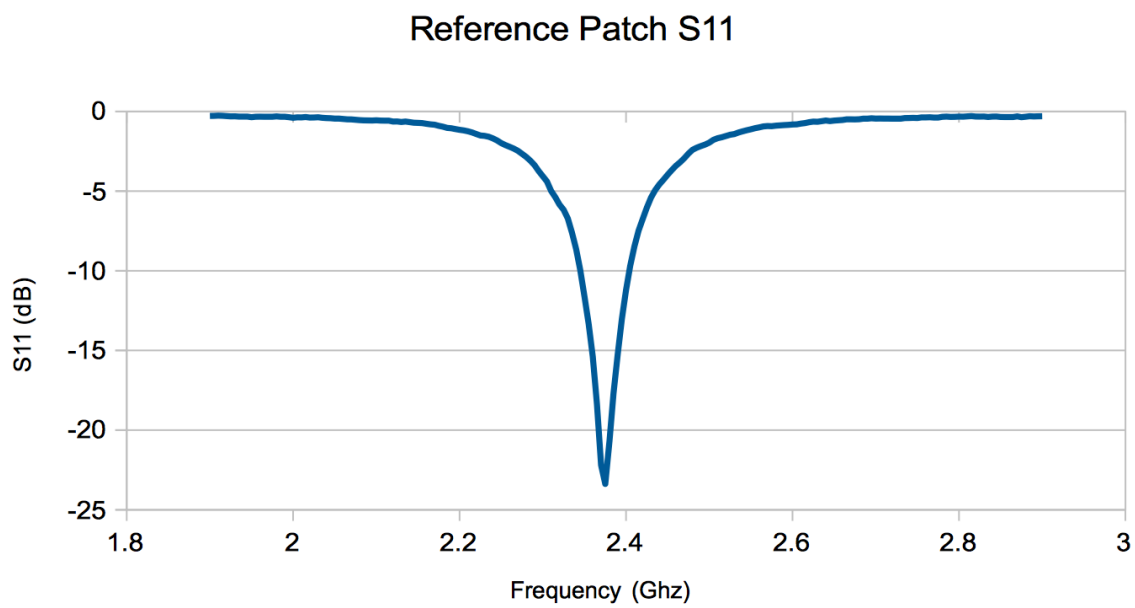


Fig. 6.17: Reference Patch Return Loss

The following table details additional results for the prototypes and reference patch. The directivity values were measured from the anechoic chamber and they do not account for losses (ohmic, mismatch, etc.) The estimated gain values were computed by comparing the EIRP values of each prototype antenna to the reference patch and adding the differences to the simulated reference patch gain (which is 6.5 dBi).

6.3. Results and Design Tradeoff Discussion

Table 6.2: Additional Prototype Results

Prototype Number	Directivity (dBi)	Est. Gain (dBi)	Gain Over Reference Patch (dB)	Percent Bandwidth	FLL (dB)	BLL (dB)
Ref. Patch	6.96	6.5	N/A	7.8	N/A	N/A
1	9.6	8.84	2.34	3	-18	-7.5
2	9.63	9	2.5	6	-15	-10
3	9.77	9.02	2.52	4	-11	-7.5
4	9.66	8.8	2.3	2.5	-10	-6

From the results, it can be seen that the prototypes have a gain of up to 2.5 dB over the reference patch, but designing patches this way comes with certain tradeoffs. They are as follows:

- 1.) Decreasing the width of the patch leads to a narrower but longer required feed network. This in turn leads to larger forward lobes in the resulting pattern. These lobes occur because of distribution mismatch between the radiation apertures as well as spurious feed

network radiation, and as the patch narrows, the pattern begins to be steadily overtaken by the unfavorable radiation characteristics. This means that the width of the patch should be chosen based on acceptable side lobe characteristics as well as the dimensions needed for the application.

2.) The bandwidth of the enhanced gain patches is less than that of the reference patch, no doubt because of the tuning requirements of the feed and matching networks, though, the bandwidth of prototype #2 is close to the reference patch bandwidth, but this is not a trend among the prototypes. For this reason, the topology is not ideal for applications that require a larger bandwidth, and care must be taken to ensure that the patch is tuned to the correct frequency of operation, that is, unless a wider band matching network is used. Other matching network designs are beyond the scope of this thesis however.

3.) It should be noted that the proof-of-principle designs here are substantially larger than the reference patch design. While this is simply a reality of the designs, methods for creating more compact versions of the topology can very well be developed in the future. However, full formulations for such versions are also beyond the scope of this thesis.

6.4. Conclusions

Here, the results of 4 enhanced gain patch prototypes were presented, confirming the effectiveness of the design techniques discussed in previous chapters. It was shown that gain enhancement of up to 2.5 dB over a normal patch antenna can be achieved for several varied designs. The next chapter will summarize the methods discussed in this thesis and touch on future research directions.

7. CONCLUSIONS AND FUTURE WORK

In this thesis, a novel technique for increasing the gain of patch antennas has been developed and verified. The process began with the formulation of a theoretical electric field distribution that yields a higher gain than the conventional case, and culminated in a full design workflow for creating a circuit that mimics this distribution. The process does have drawbacks, however, such as the bandwidth of the circuit, the front and back lobes, and the extra space needed to implement the designs. This means additional work needs to be done to refine the circuit design. This will be addressed in the following section.

7.1. Enhanced Gain Patch Pattern and Form Factor Refinement

The primary drawbacks of the enhanced gain patch design presented in this thesis arise from the fact that the patch is edge-fed. This is not explicitly necessary to obtain enhanced gain however. Noting this, a simulation prototype has been developed (though not yet fabricated) that obtains enhanced gain in a different way. Instead of feeding the patch directly from the edge, the source is connected (through a matching section) to a probe that excites a shorted half-wave resonator closely coupled to the patch underside. Another resonator is also placed on the other side of the patch for pattern symmetry. The somewhat sinusoidal voltage distribution on the resonator forces a similar distribution on the patch edge and the two voltage profiles combine at the radiating apertures to give rise to the modified radiation modes derived in chapter 3 if the resonators are tuned correctly. In this way, a closer representation of the theoretical framework is obtained and a cleaner pattern (one with less prominent lobes) is produced from an antenna circuit that has a smaller form factor than the ones previously presented. The general design and simulated results are pictured below. Again, the design was created for operation at 2.4 GHz:

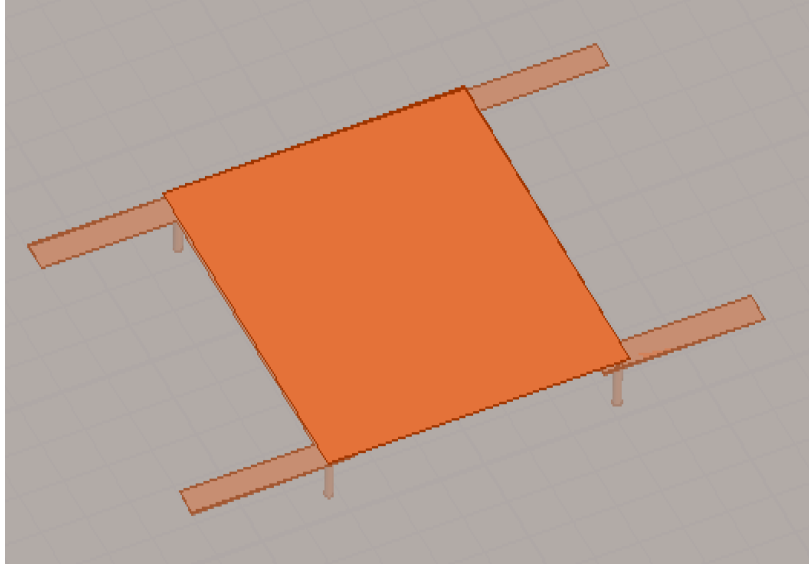


Fig. 7.1: Probe-fed prototype top view

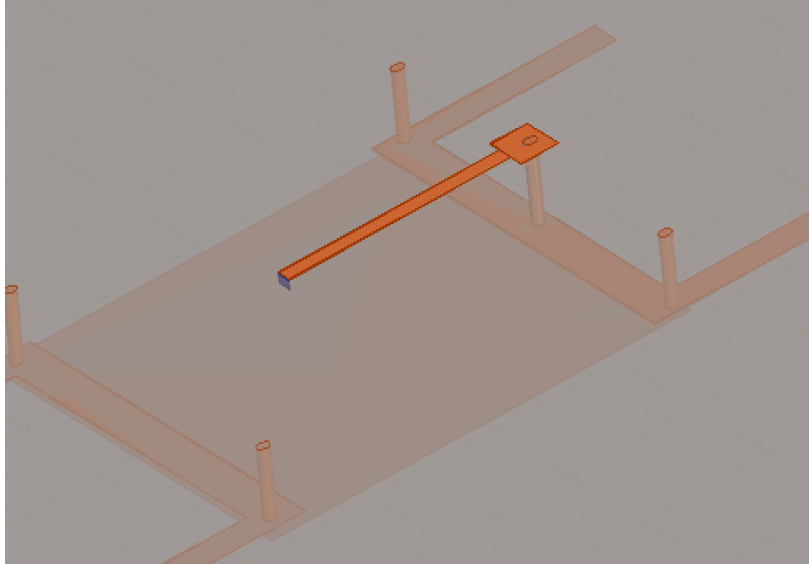


Fig. 7.2: Probe-fed prototype bottom view (quarter wave stub matching section)

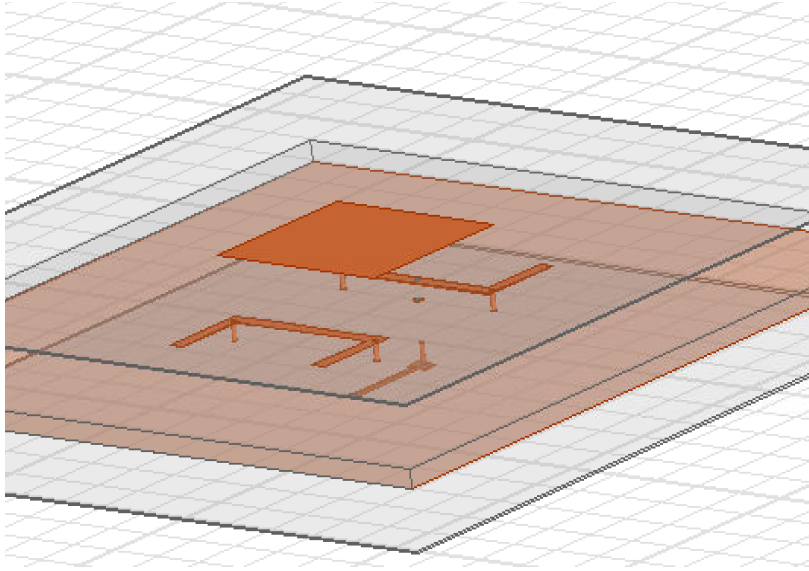


Fig. 7.3: Full design expanded view

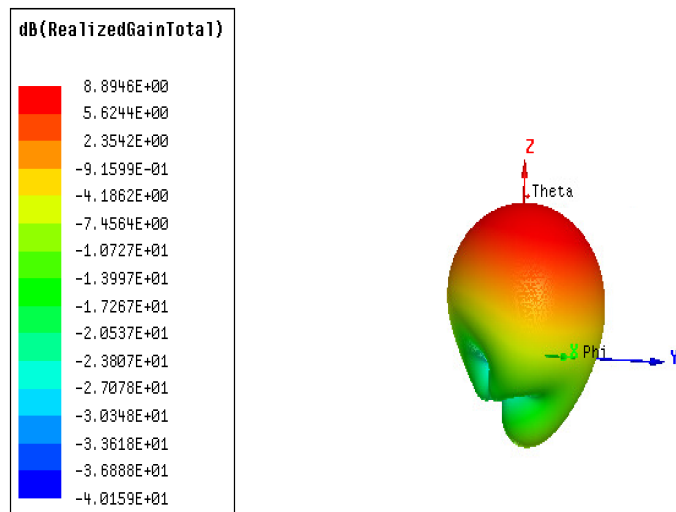


Fig. 7.4: Simulated gain pattern

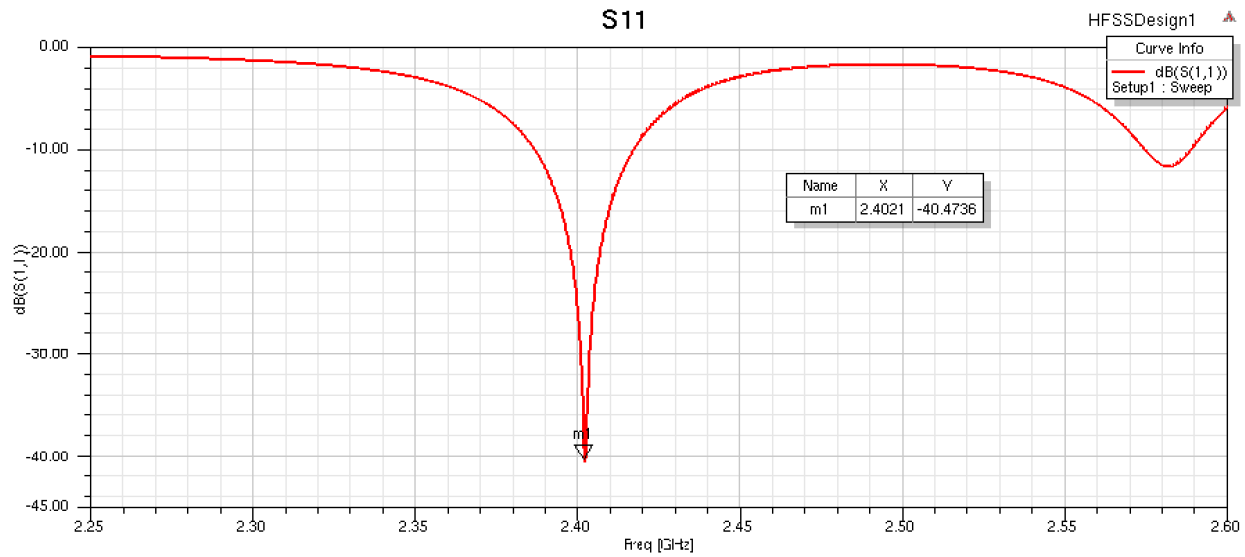


Fig. 7.5: Simulated return loss

As can be seen from the figures, the design above is far more compact than the designs presented thus far. Further, the front and back lobes disappear. There is a lobe facing downward, however, but this lobe is about -20 dB down from the maximum gain direction, so it is still a step up from the lobes of previous designs. For comparison, the simulated peak gain of prototype #4 (which has the same patch dimensions as the prototype pictured above) is 8.4 dB and the simulated gain of the reference patch is 6.5 dB, meaning the refined design outperforms previous iterations and the reference patch. This, however, comes at the cost of fabrication simplicity, as the refined design utilizes vias and three separate substrates (one 3.18mm substrate sandwiched between two 0.318mm substrates.) It should be noted that the full design process and limitations have not yet been defined, but they should be in the near future. In the next section, the concept of using the techniques of this thesis regarding alternate antenna topologies is discussed.

7.2. Other Antenna Types

Although microstrip patch antennas were the focus of this thesis, other antenna topologies could very well be enhanced using the techniques presented here, especially ones where alternate modal distributions can be developed and synthesized. The approach to be used for other antennas would be based around discovering these modal distributions that enhance the gain, and then modifying boundary conditions (via applying a specialized feed network or parasitics) to achieve the corresponding pattern. Although they haven't been formally investigated here, this technique could theoretically be applied to waveguide and aperture antennas, and could certainly be applied to any ground-backed PCB antenna. The extension of the techniques of this thesis to other antenna types will likely dominate future work in this topic, as it would move the idea closer to being generalized.

7.3. Conclusions

This concludes the development of the enhanced gain patch antenna. Within this thesis, the theoretical ideology for enhancing patch antenna gain was created, followed by a full definition of the design process to achieve this enhanced gain, as well as the fabrication and measurement of prototypes that verified the theories and design processes discussed. In the future, it is the goal of the author to refine and generalize the techniques discussed here in order to maximize the applicability of these theories to real world applications from communications to wireless power transfer. Thank you for reading and I hope this report was of use to you.

LIST OF REFERENCES

LIST OF REFERENCES

- [1] S. A. Schelkunoff, "A mathematical theory of linear arrays," *The Bell System Technical Journal*, vol. 22, no. 1, pp. 80-107, 1943.
- [2] N. Yaru, "A note on super-gain antenna arrays," *Proceedings of the IRE*, vol. 33, no. 9, pp. 1081-1085, 1951.
- [3] Yaghjian, A. D., T. H. O'Donnell, E. E. Altshuler, and S. R. Best, "Electrically small supergain end-fire arrays," *Radio Sci.*, vol. 43, RS3002, doi: 10.1029/2007RS003747, 2008.
- [4] R. P. Haviland, "Supergain antennas: possibilities and problems," *IEEE Antennas and Propagation Magazine*, vol. 37, no. 4, pp. 13-26, 1995.
- [5] H. J. Riblet, "Note on the maximum directivity of an antenna," *Proceedings of the IRE*, vol. 36, no. 5, pp. 620-623, 1948.
- [6] C. A. Balanis, "Microstrip Antennas," in *Antenna Theory Analysis and Design*, 3rd ed. Hoboken, New Jersey: Wiley, 2005, pp. 826-843.
- [7] D. M. Pozar, "Impedance and Admittance Matrices," *Microwave Engineering*, 4th ed. Hoboken, New Jersey: Wiley, 2012, pp. 174-175.

APPENDICES

A. AMPLITUDE RATIO DIRECTIVITY PLOT CREATION CODE

```

theta = linspace(0, pi, 500); %theta angle definition

t_step = theta(2) - theta(1); %step-size between theta values

phi = linspace(0, pi, 500); %phi angle definition

p_step = phi(2) - phi(1); %step-size between phi values

t = 0; %single theta value

p = 0; %single phi value

A010 = 1;

A010_prime = 1;

f = 2.4e9; %freq

lambda = 3e8/f; %wavelength

w = 2*pi*f; %omega

W = 3*.0125; %patch width

L = .035; %patch length

h = .00318; %height

ko = w/(3e8); %free space wavenumber

er = 3.27; %relative permittivity

e_eff = (er+1)/2 + ((er-1)/2)/sqrt(1+12*(h/W)); %effective permittivity

dL = (.412*h)*((e_eff + .3)*(W/h + .264))/((e_eff-.258)*(W/h + .8)); %electrical length
correction

```



```
L = L + 2*dL %effective patch length

lambda_eff = lambda/(sqrt(e_eff)); %effective patch wavelength

k = 2*pi/lambda_eff; %effective wavenumber

%parameter initializations

Directivity_array = []; %directivity values

ratio_array = []; %ratio values

ratio = .1;

%distance step size initialization

r_step = 1.9/199;

sum = 0; %numerical integration parameter

Prad = 0; %radiated power variable

D_array_count = 1; %directivity array indexing variable

Den_max = 0; %power density variable

eta = 120*pi; %intrinsic impedance of free space

%no exponentials with r included because they drop out in the power
%calculation

%this loop evaluates the directivity for amplitude ratio values between .1
%and 2

while ratio <= 2

    %normalized amplitude coefficient initialization
```

```

A010 = 1/(h*w);

A010_prime = A010*ratio;

%theta and phi integration variables

t = 0;

p = 0;

%this loop numerically computes the radiated power integral using eqns
%3.13 a-e

while t <= theta(500)

    while p <= phi(500)

        Z = .5*ko*W*cos(t);

        %edge case compensation

        if exp(j*ko*h*cos(p)*sin(t)) == 1

            X = 1;

        else

            X = (exp(j*ko*h*cos(p)*sin(t)) - 1)/(j*ko*cos(p)*sin(t));

        end

        Y = W*ko*cos(t)/2;

        AF = 2*cos(ko*L*sin(t)*sin(p)/2); %array factor

        E010 = ((ko*W*w*A010)/pi)*sin(t)*(sin(Z)/Z)*.5*AF*X; %eqn. 3.13a plus
        array factor

        E010_prime = -j*ko*((2*w*A010_prime*sin(t)*j*X)/(W*( (ko^2)*(cos(t))^2 -
        (pi^2)/(W^2))))*cos(Y)*AF; %eqn. 3.13b plus array factor
        %integration kernal and sum iteration

```

```

kernal = sin(t)*abs(E010+E010_prime)^2/(2*eta);

sum = sum + kernal*p_step*t_step;

p = p + p_step;

end

t = t + t_step;

p = 0;

end

Prad = sum %radiated power

sum = 0;

%computation of power density in desired maximum radiation direction

p = 0;

t = pi/2;

Z = .5*ko*W*cos(t);

X = (exp(j*ko*h*cos(p)*sin(t)) - 1)/(j*ko*cos(p)*sin(t));

Y = W*ko*cos(t)/2;

AF = 2*cos(ko*L*sin(t)*sin(p)/2);

E010 = ((ko*W*w*A010)/pi)*sin(t)*.5*AF*X;

E010_prime = -j*ko*((2*w*A010_prime*sin(t)*j*X)/(W*((ko^2)*(cos(t))^2 - (pi^2)/(W^2))))*cos(Y)*AF;

Den_max = abs(E010+E010_prime)^2/(2*eta);

%directivity value computation saved into directivity array

```

```
Directivity_array(D_array_count) = 10*log10(4*pi*Den_max/Prad)

ratio_array(D_array_count) = ratio;

D_array_count = D_array_count + 1;

t = 0;

p = 0;

ratio = ratio + r_step;

end

%final plot

plot(ratio_array, Directivity_array);

%code appendix to be used to quickly compute voltage ratio from the graphically ex-
tracted
%amplitude ratio value

ratio = .7;

V_ratio = (1+ratio)/(1+(ratio/2))
```

B. FEED NETWORK SYNTHESIS CODE

%Mutual Impedance Definition

Z11 = 9.6875 +1.9498.*i;

Z12 = 8.8658 -51.222.*i;

Z13 = 7.2193 -51.211.*i;

Z21 = Z12;

Z22 = 9.4576 -.32724.*i;

Z23 = Z21;

Z31 = Z13;

Z32 = Z23;

Z33 = Z11;

%Desired normalized voltage definition

V1 = 1;

V2 = .7;

V3 = 1;

%Desired current definition (this step computes the corresponding currents
%that arise from the Z-Paramters and desired voltages)

V0 = [V1, V2, V3];

Z = [Z11, Z12, Z13; Z21, Z22, Z23; Z31, Z32, Z33];

```
Z_inverted = inv(Z);
```

```
I = Z_inverted*V0';
```

```
I1 = I(1);
```

```
I2 = I(2);
```

```
I3 = I(3);
```

```
%DPI definition
```

```
r = I1./I2;
```

```
q = I1./I3;
```

```
m = I2./I3;
```

```
Z1d = Z11 + (Z12)./r + (Z13)./q
```

```
Z2d = Z22 + (Z21).*r + (Z23)./m
```

```
Z3d = Z33 + (Z32).*m + (Z31).*q
```

```
%Additional variable initialization
```

```
step_deg = 90./299; %Electrical length increment step-size
```

```
Zo1 = 100; %Initial characteristic impedance
```

```
Zo2 = 100;
```

```
Zo3 = 100;
```

```
Z_step = 65/49; %Characteristic impedance step size
```

```
min_percent = 100; %tolerance variable definition
```

```
%Guess-and-Check loop. Conditions for loop exit: characteristic impedances
%reach 150 Ohms or minimum percent tolerance (.5%) has been achieved.
%Electrical lengths varied between 0 and 180 degrees
```

```
while Zo2 <= 150 && min_percent >= .5
```

```
    while Zo1 <= 150 && min_percent >= .5
```

```
        e2 = 0;
```

```
        while e2 <= 180
```

```
            e2_r = pi.*e2./180; %Convert electrical length from degrees to radians
```

```
            gamma = (Z1d-Zo1)./(Z1d+Zo1); %Line reflection coefficient definition
```

```
            gamma2 = (Z2d-Zo2)./(Z2d+Zo2);
```

```
            step = 2.*pi./99;
```

```
            e = 0;
```

```
            min = 100;
```

```
            minlength = 0;
```

```
            checkval = 0;
```

```
            while e >= -pi
```

```
                %evaluation of port current ratio with current parameters
```

```
                %and subtraction of desired current ratio from this value.
```

```
                %if the magnitude of "check" is low, a solution close to
```

```
                %the desired distribution has been found. the equation is a
```

```

%direct result of Eqn. 4.6a

check = ((1+gamma).*Z2d.*exp(i.*e2_r).*(1+gamma2.*exp(-2.*i.*e2_r)))/
        ( Z1d.*exp(-i.*e).*(1+gamma.*exp(2.*i.*e)).*(1+gamma2) ) - r;

%statement to save current parameters if they provide the
%most optimal solution computed thus far in the iteration
%cycle

if abs(check) < min

    abs(check);

    minlength = e;

    checkval = check;

    min = abs(check);

end

e = e - step;

end

%outputs for tracking program progress

min;

checkval;

electrical_length1 = -180.*minlength./pi;

r;

%computation of percent error for current optimum solution

accuracy1 = ((1+gamma).*Z2d.*exp(i.*e2_r).*(1+gamma2.*exp(-2.*i.*e2_r)))/
            ( Z1d.*exp(-i.*minlength).*(1+gamma.*exp(2.*i.*minlength)).*(1+gam-
ma2) );
percent_error1 = 100.*(abs(r-(accuracy1))./abs(r));

```


%if the current percent error is the smallest error found thus
%far, the input impedance of the circuit is evaluated

if abs(percent_error1) < min_percent

e1_rad = pi*electrical_length1/180;

e2_rad = e2_r;

Zin1 = Zo1*((Z1d + i*Zo1*tan(e1_rad))/(Zo1+i*Z1d*tan(e1_rad)));

Zin2 = Zo2*((Z2d + i*Zo2*tan(e2_rad))/(Zo2+i*Z2d*tan(e2_rad)));

Zin_tot = ((Zin1/2).*Zin2)/(Zin1/2+Zin2);

%here the input impedance is looked at by the following
%"if" statement. If the resistance and reactance are
%within user-defined ranges, the current transmission line
%parameter set will be saved. otherwise, the current set
%will be ignored.

if real(Zin_tot) >= 5 && abs(imag(Zin_tot)) <= 100 && real(Zin_tot) <= 100

electrical_length1_final = electrical_length1;

electrical_length2_final = e2;

accuracy_final1 = accuracy1;

Zo1_final = Zo1;

Zo2_final = Zo2;

min_percent = percent_error1

percent_error_final1 = percent_error1;

Zin_tot_save = Zin_tot;

```
        end

    end

    e2 = e2 + step_deg;

end

    Zo1 = Zo1+Z_step;

end

    Zo2 = Zo2+Z_step

    Zo1 = 100;

end

%the following statements extract the final parameters

    e = -pi*electrical_length1_final/180;

    min_percent = 100;

    min = 100;

    e1_r = pi*electrical_length1_final/180;

    e2_r = pi*electrical_length2_final/180;

%if statement to account for symmetry

if I1 == I3

    Zo1_f = Zo1_final;

    Zo2_f = Zo2_final;
```

```
Zo3_f = Zo1_final;  
  
accuracy_final2 = accuracy_final1;  
  
percent_error_final2 = percent_error_final1;  
  
e_length_f1 = 180*e1_r/pi;  
  
e_length_f2 = 180*e2_r/pi;  
  
e_length_f3 = e_length_f1;  
  
else  
  
    Zo1_f = Zo1_final;  
  
    Zo2_f = Zo2_final;  
  
    Zo3_f = Zo1_final;  
  
    accuracy_final2 = accuracy_final1;  
  
    percent_error_final2 = percent_error_final1;  
  
    e_length_f1 = 180*e1_r/pi;  
  
    e_length_f2 = 180*e2_r/pi;  
  
    e_length_f3 = e_length_f1;  
  
end  
  
%final outputs  
  
min_percent  
  
r  
  
accuracy_final1  
  
percent_error_final1
```

m

accuracy_final2

percent_error_final2

Zo1_f

e_length_f1

Zo2_f

e_length_f2

Zo3_f

e_length_f3

Zin_tot_save